ISTANBUL TECHNICAL UNIVERSITY ★ GRADUATE SCHOOL OF SCIENCE
ENGINEERING AND TECHNOLOGY

SIMULTANEOUS
SCANNING TUNNELING/ATOMIC FORCE MICROSCOPY
INVESTIGATION OF DIAMOND SURFACES IN ULTRA HIGH VACUUM

M.Sc. THESIS

İpen DEMİREL

Department of Physics Engineering

Physics Engineering Programme

SEPTEMBER 2018

ISTANBUL TECHNICAL UNIVERSITY ★ GRADUATE SCHOOL OF SCIENCE ENGINEERING AND TECHNOLOGY

**SIMULTANEOUS
SCANNING TUNNELING/ATOMIC FORCE MICROSCOPY
INVESTIGATION OF DIAMOND SURFACES IN ULTRA HIGH VACUUM**

M.Sc. THESIS

**İpen DEMİREL
(509161110)**

Department of Physics Engineering

Physics Engineering Programme

Thesis Advisor: Assoc. Prof. Hakan Özgür ÖZER

SEPTEMBER 2018

ISTANBUL TEKNİK ÜNİVERSİTESİ ★ FEN BİLİMLERİ ENSTİTÜSÜ

ELMAS YÜZEYLERİN EŞZAMANLI TARAMALI TÜNELLEME/ATOMİK KUVVET MİKROSKOBU İLE ULTRA YÜKSEK VAKUMDA İNCELENMESİ

YÜKSEK LİSANS TEZİ

İpen DEMİREL
(509161110)

Fizik Mühendisliği Anabilim Dalı

Fizik Mühendisliği Programı

Tez Danışmanı: Doç. Dr. Hakan Özgür ÖZER

EYLÜL 2018

İpen Demirel, a M.Sc. student of İTU Graduate School of Science Engineering and Technology student ID 509161110, successfully defended the thesis/dissertation entitled "SIMULTANEOUS SCANNING TUNNELING/ATOMIC FORCE MICROSCOPY INVESTIGATION OF DIAMOND SURFACES IN ULTRA HIGH VACUUM", which she prepared after fulfilling the requirements specified in the associated legislations, before the jury whose signatures are below.

Thesis Advisor :   **Assoc. Prof. Hakan Özgür ÖZER**   ....
İstanbul Technical University

Jury Members :   **Assoc. Prof. Hakan Özgür ÖZER**   ....
Istanbul Technical University

              Prof. Ferid SALEHLİ   ....
Istanbul Technical University

              Dr. Doğuş ÖZKAN   ....
Milli Savunma Üniversitesi

Date of Submission : 5 September 2018
Date of Defense   : 21 September 2018

To my mother and father,

FOREWORD

I would like to express my deepest appreciation to my supervisor Assoc. Prof. H. Özgür ÖZER for his guidance and endless support, during all the time I had at Nanomechanics Lab, and above all giving me the opportunity to participate in his group.

I appreciate Prof. Mustafa ÜRGEN for sharing his precious thoughts, sources and samples. I would also like to thank NanoMagnetics Instruments and Adama Innovations for providing technical supply.

I would like to express my gratitude to Majid Fazeli Jadidi for his assistance and motivation. I would like to thank Ahmed Uluca for his help and support.

I would like to thank my close friends for their support.

I am deeply grateful to my beloved mother and father, who I owe everything I have achieved in my life, for always being there for me.

September 2018   İpen DEMİREL

TABLE OF CONTENTS

ABBREVIATIONS

STM : Scanning Tunneling Microscopy

AFM : Atomic Force Microscopy

SPM : Scanning Probe Microscopy

UHV : Ultra High Vacuum

CVD : Chemical Vapor Deposition

MW-CVD : Microwave Chemical Vapor Deposition

HF-CVD : Hot Filament Chemical Vapor Deposition

SYMBOLS

Å	**:** Ångström
nA	**:** nanoAmper
z	**:** Tip-surface distance
V	**:** Volt
p-p	**:** peak to peak
V_{bias}	**:** Bias voltage
I_t	: Tunnel current
A_0	**:** Free oscillation amplitude
ω_0	**:** Resonance frequency
ω	**:** Excitation frequency
ϕ	**:** Barrier height
k	**:** Stiffness
W	**:** Tungsten
Hz	**:** Hertz
κ	**:** Decay constant
K	**:** Kelvin

LIST OF FIGURES

SIMULTANEOUS SCANNING TUNNELING/ATOMIC FORCE MICROSCOPY INVESTIGATION OF DIAMOND SURFACES IN ULTRA HIGH VACUUM

SUMMARY

Diamond has always been one of the most outstanding naturally existing materials due to its distinguishing thermal and mechanical properties. As it is known as the hardest material, diamond has been a field of interest in plenty of mechanical studies and has taken its place in industry for different uses, as well. In the last few decades, with the pursuit of adaptation of semiconductors to the technology, the search for more durable novel materials with manipulative electronic characteristics has ascended. Thus, diamond has been one of the most popular research areas, such as the synthesis processes and surface studies, including scanning probe microscopy. Atomic Force Microscopy (AFM) studies of both natural and CVD grown diamond surfaces revealed the topography of diamond surfaces with different surface orientations and reconstructions. Besides, Scanning Tunneling Microscopy (STM) studies of diamond have shown that the electronic structure of diamond is highly related to the type of dopants and surface termination. In this study, the diamond surface has been investigated using simultaneous Scanning Tunneling/Atomic Force Microscopy in ultra-high vacuum (UHV).

The investigation of diamond using simultaneous STM/AFM in UHV has been focused on polycrystalline and single crystalline diamond surfaces. The cleaning techniques including the sputtering, annealing and acid etch have also been practiced, in order to obtain atomically clean and flat diamond surfaces. The simultaneous STM/AFM system used in this study operates as using the tunnel current as the feedback parameter. By oscillating the cantilever at a specific frequency well below its resonance frequency, oscillations with sub-Ångström amplitudes were obtained. The detection of such small cantilever oscillation amplitudes was enabled by using a fiber-optic interferometry setup. Scanning the surfaces using such small cantilever oscillation amplitudes enables the true simultaneous STM/AFM operation on the diamond surfaces, by the means of being at certain operating regimes while scanning the surface. With the simultaneous STM/AFM system used in this study, surface topography, force, interaction stiffness, tunnel current modulation (measure of barrier height), phase shift (energy dissipation) and tunneling current were obtained. In this study, the diamond surfaces were scanned using two different cantilevers, a Tungsten (k=53 N/m) and a highly boron doped diamond cantilever (k=70 N/m), which were calibrated using thermal noise method. Atomic resolution imaging of different regions on diamond surfaces was achieved.

Moreover, force-distance spectroscopies were conducted on different regions on the diamond surfaces, leading to obtain the interaction stiffness between the diamond and the tip. The maximum negative interaction stiffness between the polycrystalline diamond surface and the W tip is measured around -2-2.5 N/m, where the interaction

stiffness between the polycrystalline diamond surface and the highly boron doped diamond tip is measured as -1.2 N/m. For the single crystalline diamond, the maximum negative interaction stiffness between the sample surface and the W tip is measured as -2.5 N/m and -1.2 N/m, with an applied bias voltage of -1 V and 1 V respectively. The maximum negative interaction stiffness between the single crystalline surface and the highly boron doped diamond tip is measured as -1.5 N/m.

ELMAS YÜZEYLERİN EŞZAMANLI TARAMALI TÜNELLEMELİ/ATOMİK KUVVET MİKROSKOBU İLE ULTRA YÜKSEK VAKUMDA İNCELENMESİ

ÖZET

Elmas doğal olarak var olan karbon bazlı malzemelerden biridir. Tetrahedral olarak bağlanmış karbon atomlarından oluşur ve örgü sabiti 3.57 Å'dur. Elmas keşfedildiğinden beri, nadiren bulunan bir malzeme olması sayesinde kültürler için her zaman değerli bir taş olmuştur. Bunun yanısıra, elmas ayırtedici termal ve mekanik özellikleri sayesinde doğada bulunan malzemeler arasında daima farklı bir yere sahip olmuştur. Varolan en sert malzeme olarak bilinen elmas, böylelikle bir çok mekaniksel çalışma alanında ve endüstride de yerini almıştır.

Son yıllarda, yarıiletken malzemelerin teknolojiye adapte edilmesi amacıyla, manipüle edilebilir elektronik özelliklere sahip, daha dayanıklı malzemeler bulma arayışı başladı. Böylece elmas, Taramalı Uç Mikroskobu (TUM) da dahil olmak üzere, sentezlenme süreci ve yüzey çalışmaları gibi alanlarda daha detaylı çalışılmaya başlanmıştır. Bu zamana kadar yapılan Taramalı Uç Mikroskobu çalışmalarında elmasın çeşitli özellikleri incelendi. Taramalı Uç Mikroskobu teknikleri ile elmas yüzey çalışmalarına olan ilgi; yüzey topografisi, malzemenin elektronik özellikleri, elmas yüzeyinin sürtünme karakteristikleri de dahil olmak üzere genel yüzey yapısına ışık tutmaktadır.

İlk zamanlarda Atomik Kuvvet Mikroskobu ile çoğunlukla elmasın mekanik özellikleri üzerine daha detaylı çalışmalar yapıldı. Doğal olarak bulunan ve Kimyasal Buhar Biriktirme yöntemi ile elde edilen elmas yüzeyler üzerinde yapılan Atomik Kuvvet Mikroskobu (AKM) çalışmaları, farklı yüzey yönelimleri ve yapılanmalarına sahip yüzeylerin topografilerinin elde edilmesini sağladı. Bunun yanında, elmas üzerinde yanal kuvvet mikroskobisi de dahil olmak üzere daha detaylı sürtünme kuvveti çalışmaları da yapıldı.

Daha sonralarda ise farklı malzemelerle katkılanmış elmasın elektronik özelliklerinin değiştiği gözlemlendi ve Taramalı Tünelleme Mikroskobu kullanılarak yüzeyin elektronik yapısını inceleyen çalışmalar yapılmaya başlandı. Elmas üzerine yoğunlaşan çalışmalar, elmasın sentetik olarak üretilmesi üzerine geliştirilen yöntemlerle de artmıştır. Kimyasal buhar biriktirme (KBB) yöntemi ile yüksek basınç/yüksek sıcaklıkta farklı parametreler ve katkı malzemeleri kullanılarak, istenilen yönelimde monokristal ya da polikristal elmas üretilmeye başlandı. Böylece, kullanılma amacına yönelik olarak üretilen elmasın elektronik özelliklerini ve yönelimini belirlemek mümkün oldu. Elmasın topografisi, büyüme mekanizması ve grafitizasyonu üzerine odaklanan çalışmaların yanı sıra, elmasın yüzey yapısının atomik çözünürlükte görüntülemesini içeren çalışmalar da mevcuttur.

Bu çalışmada, elmas yüzeyi daha geniş bir perspektiften incelenerek, ultra yüksek vakum (UYV) ortamında eşzamanlı Taramalı Tünelleme/Atomik Kuvvet Mikroskobu kullanılarak çalışılmıştır. UYV ortamında eşzamanlı TTM/AKM

kullanılarak polikristal ve monokristal elmas yüzeylere odaklanılmıştır. Atomik olarak temiz ve düz elmas yüzeylerin elde edilmesi için, iyon bombardımanı, tavlama ve kimyasal olarak asitle temizleme teknikleri uygulanmıştır. Temizleme teknikleri farklı parametreler kullanılarak gerçekleştirilmiş ve bu tekniklerin yüzey üzerindeki etkisi incelenmiştir. Daha sonrasında örnekler eşzamanlı TTM/AKM ile incelenmiştir.

Bu çalışmada kullanılan eşzamanlı TTM/AKM sistemi, geri besleme parametresi olarak tünel akımını kullanmaktadır. AKM yayının rezonans frekansının çok altında belirli bir frekansta salındırılmasıyla, Ångström-altı salınım genlikleri elde edilmiştir. Bu mertebedeki yay salınım genliklerinin saptanması, fiber-optik interferometre düzeneği kullanılarak gerçekleştirilmiştir.

Fiber-optik interferometre yöntemi temel olarak Fabry-Perot interferometresine benzer. Bir lazer diyotun ikiye ayrılarak referans fotodiyota ve fibere gönderilmesiyle oluşur. Fiber içinde ilerleyen ışınların bir kısmı fiberin ucundan geri yansırken, bir kısmı da ilerleyerek fiberin ucunun olabildiğince yakınına hizalanmış yayın arkasından yansıyarak fiberin içine geri döner. Böylece sinyal fotodiyotta bir girişim deseni oluşur. Girişim deseni üzerinde eğimin (mV/Ångström) en yüksek olduğu nokta ise fiber-optik interferometre sisteminin hassasiyetini belirler ve fiber bir tüp piezo yardımıyla girişim deseni üzerindeki en hassas noktada kilitlenir. Böylece tarama sırasında yayın salınımının Volt değerinden Ånström değerine çevrilerek mesafe olarak elde edilmesi mümkün olmaktadır.

Elmas yüzeylerin Ångström-altı mertebede salınım genlikleri kullanılarak taranması, tarama sırasında belirli bir etkileşim bölgesinde kalabilmeyi ve böylece yüzeyler üzerinde gerçek eşzamanlı TTM/AKM çalışılmasını sağlar. Bu çalışmada kullanılan eşzamanlı TTM/AKM sistemi ile elmas yüzeyinde topografi, kuvvet, kuvvet etkileşimi, tünel akımı modülasyonu, faz kayması (enerji kaybı) ve tünel akımı ölçümleri elde edilmiştir.

Bu çalışmada, elmas yüzeyler Tungsten (k=70 N/m) ve yüksek bor katkılı elmas (k=53 N/m) olmak üzere, iki farklı AKM yayı ile taranmıştır. Atomik Kuvvet Mikroskobu sisteminde yüzey ve iğne arasındaki etkileşimin doğru olarak ölçülebilmesi için kullanılan yayın mekanik özelliklerini bilmek büyük bir önem taşır. Yay sabiti, rezonans frekansı, kalite faktörü gibi özellikleri çeşitli yöntemler kullanarak kalibre etmek mümkündür. Bu çalışmada yay sabitlerinin kalibrasyonu termal gürültü yöntemi kullanılarak kalibre edilmiştir.

Yayın hiç bir uyarı sinyali uygulanmadan alınan frekans spektrumuyla termal rezonans genliği elde edilir. Eşbölüşüm teoreminden yola çıkarak elde edilmiş Brownian gürültü ifadesi kullanılarak yay sabiti için yaklaşık bir ifade elde edilmeye çalışılmıştır. Bu yöntemle kullanılan yayın sertlik ve kalite faktörü elde edilebilir. Bu çalışmada, elmas yüzeylerde farklı bölgelerde atomik çözünürlükte görüntüler elde edilmiştir.

Atomik Kuvvet Mikroskobu presibinde iki atom arasındaki kuvvet etkileşimi önemli bir niceliktir. Buradan yola çıkarak, bu çalışmada elmas yüzeyindeki C atomu ile tarama sırasında kullanılan yayın ucundaki C atomu arasındaki kuvvet etkileşiminin sayısal olarak ölçümü üzerinde yoğunlaşılmıştır. Çeşitli elmas yüzeyleri üzerinde belirli noktalarda kuvvet-mesafe spektroskopileri yapılarak, kuvvet etkileşimi noktasal olarak ölçülmüştür.

Polikristal elmas yüzeyi ile W iğne arasındaki maksimum negatif etkileşim sertliği -2-2.5 N/m civarında ölçülmüştür. Polikristal elmas yüzeyi ve yüksek bor katkılı elmas iğne arasındaki etkileşim sertliği ise -1.2 N/m olarak ölçülmüştür. Monokristal elmas için, örnek yüzeyi ve W iğne arasındaki maksimum negatif etkileşim sertliği örnek yüzeyine -1 V bias voltaj uygulandığı durum için -2.5 N/m, 1 V uygulandığı durum için ise -1.2 N/m olarak ölçülmüştür. Monokristal yüzey ve yüksek bor katkılı elmas iğne arasındaki maksimum negatif etkileşim sertliği -1,5 N/m olarak ölçülmüştür.

1. INTRODUCTION

The discovery of diamond lasts thousands of years ago. It has always been attractive, since it is a rarely found material with a spectacular appearance. For centuries, it has been one of the most valuable jewels. For the last few decades, diamond has taken attention not only because of its unique appearance, but also due to its remarkable thermal and mechanical characteristics. These characteristics include high thermal conductivity and physical rigidity, as well as various optical properties due to the impurities. Considering natural diamonds, these impurities arise from the formation conditions of the diamond. Later on, it has been understood that these impurities have a huge impact on both the optical and electronic properties of the diamond.

Consequently, scientists tried to find a way to produce this rarely found precious material synthetically in laboratory conditions. With the improvement of the synthesis of diamond by Chemical Vapor Deposition (CVD), the interest on the diamond surface has increased even further. The ability to grow diamond surfaces by CVD led to an increase in the adaptation of diamond in the industrial applications. Thus, the properties of CVD grown diamond depending on the formation conditions were investigated further in surface studies, including Scanning Probe Microscopy (SPM).

The Atomic Force Microscopy and Scanning Tunneling Microscopy studies revealed the surface structure, mechanical and electronic properties of different types of diamonds. Besides the works focusing on the topography, growth mechanism and graphitization of diamond, the studies including the atomic resolution imaging of the surface structure of diamond emphasize mostly the effect of dopants on the electrical properties of the diamond, H-terminated and O-terminated diamond surfaces and reconstructions on different surface orientations.

1.1 Purpose of Thesis

The interest on diamond surface studies using Scanning Probe Microscopy (SPM) techniques has shed light to the surface structure in a general basis, including surface

topography, electronic properties, frictional characteristics of the diamond surface, separately. In this study, obtaining STM and AFM information on the diamond surface simultaneously, is aimed. The advantages of scanning the surface with a cantilever while using the tunnel current as a feedback, which will be discussed further on the next sections, are significant. Considering the ability to investigate the surface in a wider perspective, in the means of both STM and AFM channels, achieving surface topography, force, interaction stiffness, tunnel current modulation (measure of barrier height), phase shift (energy dissipation) and tunnel current information on diamond simultaneously, was aimed.

Arising from the point that the force interaction between two atoms is the most important quantity in the concept of AFM, the main focus in this study has been on the quantitative measurement of the force interaction between the C atom of diamond and the atom belonging to the tip used. By conducting force-distance spectroscopy at a certain point on the diamond surface, the interaction stiffness was tried to be measured locally.

In this study, using two different types of diamond samples, a polycrystalline and a single crystalline diamond, a comparative study of surface characteristics could be possible. Achieving atomic resolution imaging of different regions on these two different diamond surfaces was aimed.

1.2 Literature Review

Diamond has always been a widely known material with its outstanding thermal conductivity, physical hardness and rigidity. Besides its thermal and physical properties, there has been a large interest on diamond, focusing further on its electrical characteristics. The possibility of the growth of diamond surfaces using Chemical Vapor Deposition (CVD) provided an increase in the use of this material in the technological applications.

The studies on the surface structure of diamond including the STM and AFM are focused on different kinds of diamond surfaces. Natural and CVD grown single crystalline and polycrystalline diamond surfaces have been studied with both STM and AFM, which will be mentioned further in detail.

Diamond already exists in the nature in different colours due to the impurities it contains. As mentioned, the properties these impurities bring is not only limited with the differing colours. The changing electrical conductivity characteristics of diamond are observed in various studies. During the CVD growth process of diamond, different dopants may be implanted to the diamond structure [1]. One of the mostly used doping materials is boron, since it enables to obtain electrical conductivity and therefore makes it possible to study the diamond surface by scanning tunneling microscopy [2].

Another area of interest in the surface studies of diamond is the effect of termination of the surface with different materials, such as hydrogen and oxygen, as it plays an important role on the electrical characteristics. The termination of the diamond surface with hydrogen or oxygen changes the electrical structure of the surface, from an insulator to a p-type or n-type semiconductor [3]. The scanning tunneling microscopy studies of diamond are mostly focused on the hydrogenated and H-terminated single crystalline diamond surfaces. The reason behind this is that H treatment enables to obtain a flat and stable diamond surface.

Stallcup et. al. observed the CVD grown (100) surface by scanning tunneling microscopy in UHV and discussed the dependence of the surface topography and reconstruction structure on the surface, as seen in Figure 1.1 [4]. In this study, it is reported that the exposure of (100) surface to atomic hydrogen enables partial (2x1) reconstruction of the surface, where the surface after growth is initially amorphous. Different concentrations and durations of atomic hydrogen exposure were studied and dimerization of the (100) surface is revealed by atomic resolution images. This is explained by the fact that the atomic hydrogen etches the amorphous carbon and leads to a stable (2x1) reconstructed surface as well.
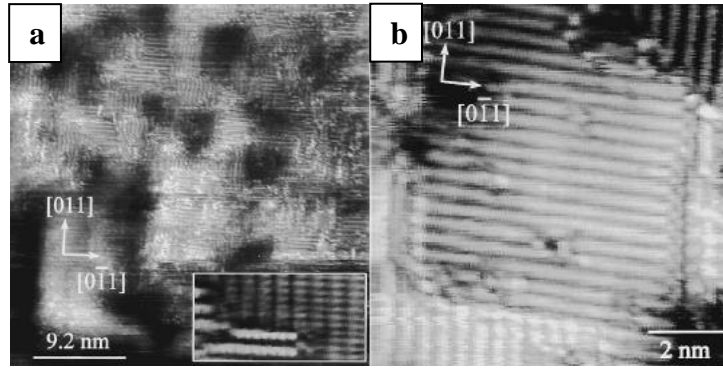
Figure 1.1 : UHV STM image of diamond (100) surface after post growth exposure to atomic hydrogen for (a) 2 min (b) 5 min [4]

The clean C(100)-(2x1) reconstructed diamond surface seen in Figure 1.2 was obtained by the dehydrogenation of the previously hydrogenated C(100)-(2x1) surface by annealing at 1000 C, as reported by Stallcup et. al. The mentioned scanning tunneling microscopy study of clean C(100)-(2x1) reconstructed surface in UHV reveals the defects and vacancies in this surface, and the atomic resolution imaging of the surface has shown that the buckling of dimers in this surface is not observed [5].
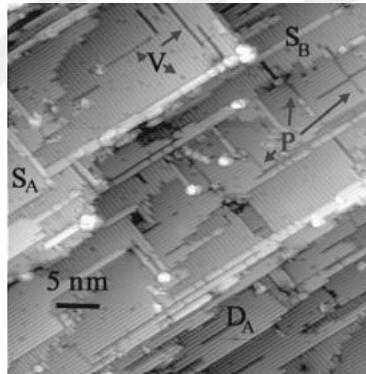
Figure 1.2 : UHV STM image of the clean C(100) 2x1 reconstructed surface [5].

Another study on the natural boron-doped single crystalline hydrogenated (100) diamond surface with the (2x1) reconstruction as seen in Figure 1.3, emphasized on the electronic properties of this surface [6]. In this study, it is argued that the hydrogenation process helps the saturation of the dangling bonds. Furthermore, the I-V spectroscopy dependence of the samples on the annealing temperature was studied, revealing that annealing leads to desorption of surface oxygen and hydrogen, which affects the electronic characteristics of the diamond.
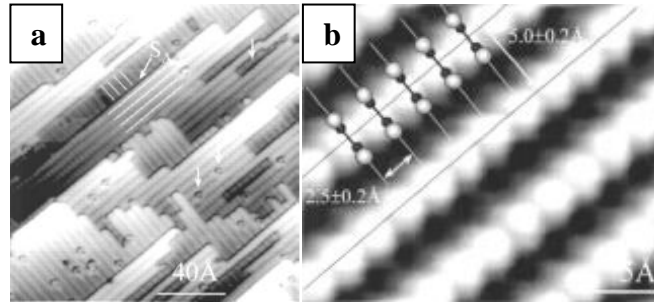
Figure 1.3 : UHV STM topography images of diamond (100) 2x1:H surface. (a) unoccupied states. (b) occupied states [6].

Tsuno et. al. studied the homoepitaxially MW-CVD grown (111) diamond surface, using scanning tunneling microscopy in ambient conditions, observing the atomic resolution imaging of (111) surface with 1x1 structure, terraces and steps, given in Figure 1.4 [7].
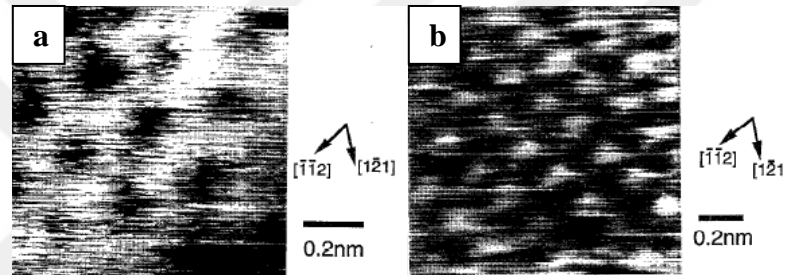
Figure 1.4 : STM topography images of diamond (111) surface grown by CVD. (a) tip bias (b) sample bias [7].

An atomic force microscopy study in ambient conditions on the polycrystalline diamond surfaces grown by HF-CVD shows different orientations of the diamond film surfaces. The atomic resolution imaging shows a periodicity of 0.35 nm in the <100> direction on (100) surface, whereas of 0.25 nm on the (111) surface [8].

Nimmrich et. al. conducted a non-contact atomic force microscopy study at room temperature UHV on type IIa diamond grown by CVD [9]. In this study, the ex-situ hydrogenated C(100)-(2x1) surface is presented in high resolution atomic images, as given in Figure 1.5. Besides, it is stated that the removal of hydrogen is possible by annealing the hydrogenated sample above 1200 K, which also enabled atomic resolution images of clean C(100)-(2x1) surface, where the distance between dimers and between rows are given as 2.50±0.05 Å and 5.10±0.08 Å respectively.
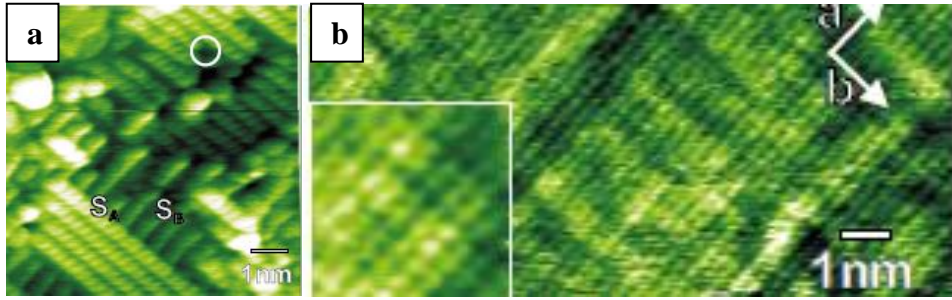
Figure 1.5 : NC-AFM images of diamond (100) 2x1:H surface (a) topography (b) frequency shift [9].

2. STM/AFM IN UHV

2.1 An Introduction to Scanning Probe Microscopy

Scanning probe microscopy techniques have brought a remarkable approach to the surface science. These techniques are based on the interaction of a sharp tip with a surface, and mainly the surface topography is obtained. With the invention of scanning tunneling microscopy in 1982 by Binnig et al., surface topography of conductive materials using a conductive probe was acquired [10]. However, scanning tunneling microscopy is a limited technique only for the conductive surfaces. The invention of atomic force microscopy by Binnig, Quate and Gerber in 1987, enabled the investigation of insulating surfaces, as well as conductive surfaces [11].

2.1.1 Scanning tunneling microscopy

In scanning tunneling microscopy, the main element is the tunneling current between the tip and the surface, due to the principle of quantum tunneling. This principle mainly states the possibility of an electron passing through an energy barrier which has a relatively higher energy, as shown in Figure 2.1 [12].
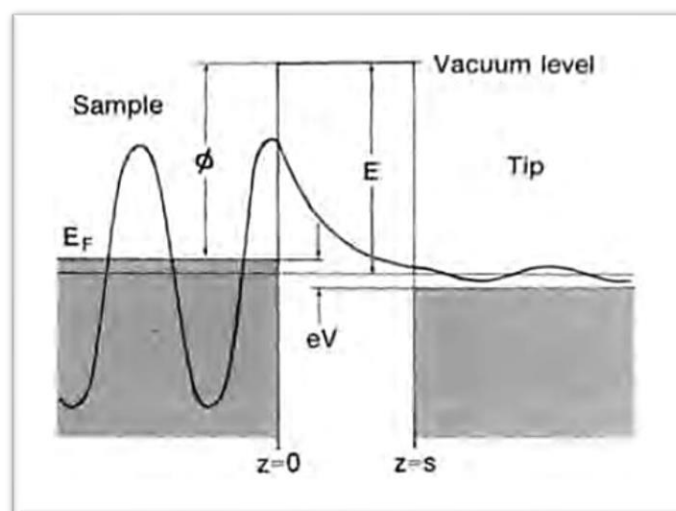
Figure 2.1 : Schematic of the quantum tunneling phenomena between the tip and sample in STM.

The application of this principle to STM is achieved by applying a bias voltage between the tip and the sample, which enables the electron flow between the tip and the surface with a very small gap in between. The electron flow, which is called tunneling current, depends on the tip-surface distance (z), the local density of states (ρ_s) and the applied bias voltage (V) is given with the equation 2.1 [12].

$$I_{tunneling} \approx \sum_{E_F-eV}^{E_F} |\Psi_n(0)|^2 e^{-2\kappa z} \approx V\rho_s(0, E_F)e^{-2\kappa z} \tag{2.1}$$

Where κ, the decay constant is expressed as a function of the work function ϕ as in equation 2.2.

$$\kappa = 0.51\sqrt{\phi(eV)} \text{ Å}^{-1} \tag{2.2}$$

Using the tunneling current, it is possible to obtain the surface topography and furthermore, the electronic characteristics of the surface. After bringing the tip and the sample to a close distance using a coarse positioner, the tunneling current is set to a specific value and used as a feedback. The surface is scanned in x and y by using a scanner piezo, which is attached to the tip and a feedback control mechanism, in order to adjust the tip-surface distance, as shown in Figure 2.2. The measurement of this tunneling current is acquired by using an I-V converter. This enables the amplification of the current and the measurement of the current in voltage.
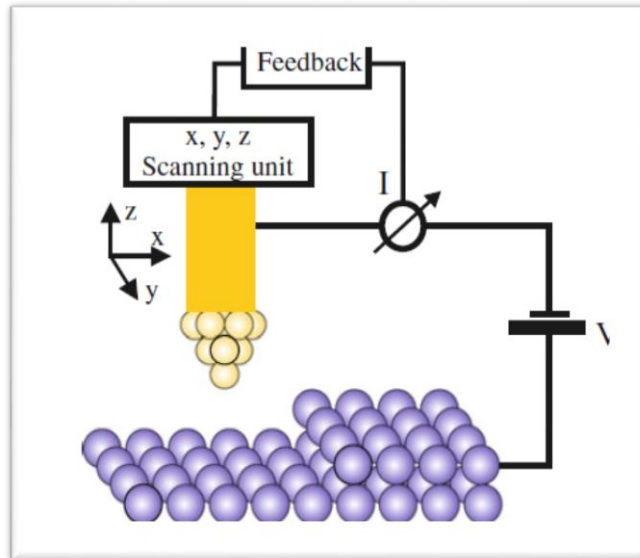
Figure 2.2 : Schematic of a typical STM setup [13].

There are two main modes of operation of STM. This depends on the set parameter that is kept constant during the scanning. When the tunneling current is used as the feedback parameter, due to the changes in the surface morphology, in order to keep the tunneling current constant, the movement of the scanner piezo in z direction maps the surface topography. This is called the constant current mode.

Another mode of operation is the constant height mode, where the tip height is kept constant. This results in a change in the tunneling current, due to the change in the tip-surface distance due to the topography and varying local density of states at different points on the surface.

2.1.2 Atomic force microscopy

The operation principle of Atomic Force Microscopy is based on the force interaction between a cantilever with a sharp probe and the surface. Interaction between the cantilever and the surface leads to the bending of the cantilever or a change in the oscillation frequency or amplitude, which is detected by using various deflection sensing techniques. The typical schematic for the operation of AFM is shown in Figure 2.3.
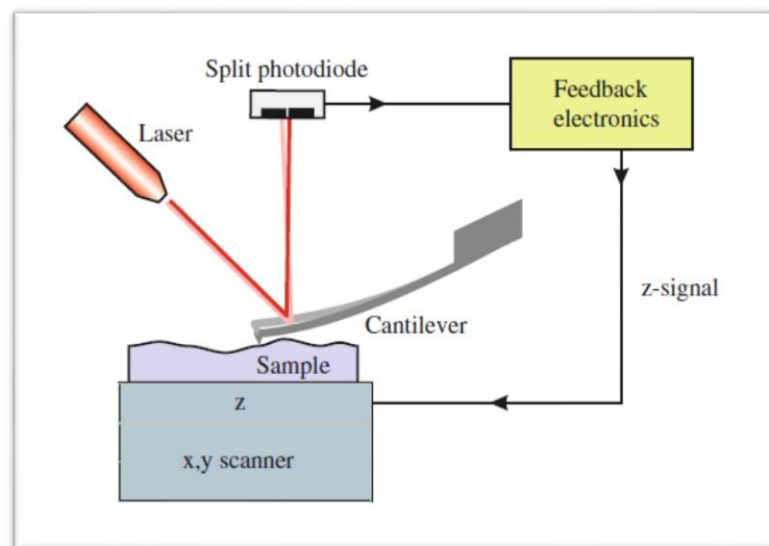
Figure 2.3 : Schematic of a typical AFM setup [13].

9

The forces measured in AFM include chemical bonding, electrostatic forces, van der Waals forces, magnetic forces, adhesion and capillary forces . In AFM, depending on the mode of operation, the effectiveness of interaction forces may differ. Due to the overlapping of the charge distributions of two atoms brought close, the electrostatic energy of the system changes. At close enough seperations, the overlap energy is repulsive due to Pauli exclusion principle [14].

When the distance between the tip and the cantilever is increased, the attractive forces become dominant. These long-range forces are attractive forces and they are more effective in distances greater than 1 nm. The van der Waals interaction is the primary attractive interaction between two atoms.

The potential energy between two atoms, depending on the distance (R) between is given by Lennard-Jones potential, which is composed of two interactions, van der Waals attraction and Pauli repulsion as expressed in equation 2.3 [15].

$$U(R) = 4\varepsilon \left[\left(\frac{\sigma}{R} \right)^{12} - \left(\frac{\sigma}{R} \right)^{6} \right]$$ (2.3)

Where ε and σ are the potential parameters. The force between two atoms is given by equation 2.4.

$$F = -\frac{dU}{dR}$$ (2.4)

The typical force distance curve between two atoms is given in Figure 2.4. The force distance curve shows the operation regimes and the behavior of force interaction depending on the distance.
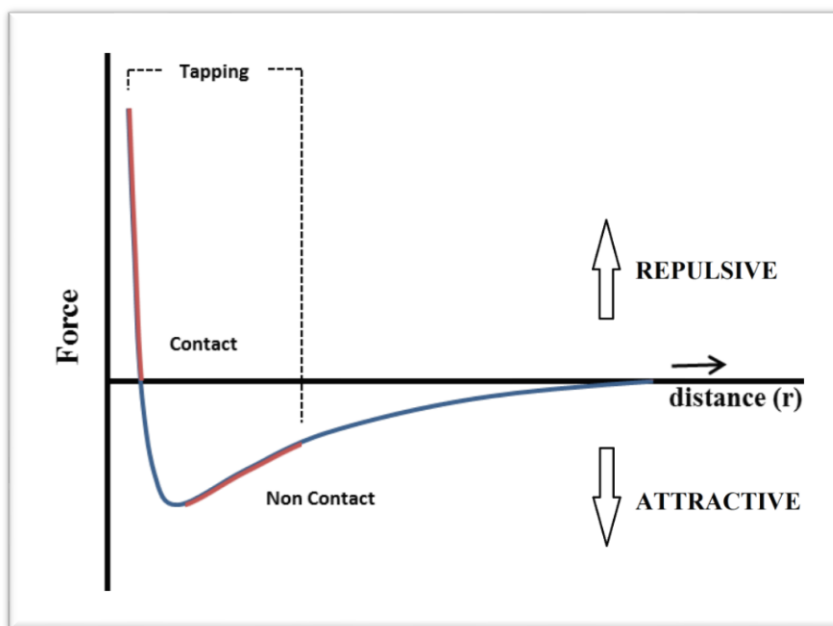
Figure 2.4 : The typical force distance curve between two atoms.

Mainly, the atomic force microscopy has three operating modes known as contact mode, tapping mode and non-contact mode. Tapping mode and non-contact mode are also classified as dynamic modes. In contact mode, the surface is scanned using a soft cantilever, while the tip is in contact with the surface. As a result of the surface topography, the deflection of the cantilever changes. By controlling the deflection of the cantilever, the surface topography is maintained. In contact mode AFM, since it is operated in short-range, the repulsive forces are dominant in a distance less than 1 nm. However, scanning the surfaced in contact mode may damage both the surface and the tip. Hence, contact mode is not preferred for delicate samples and when high resolution is desired.

In tapping mode, also known as amplitude modulation mode AFM, the cantilever is oscillated at (or close to) its resonance frequency. The approximation of the oscillation amplitude A, as a function of the driving force amplitude F_0 and the excitation frequency ω_0 is given with the equation 2.5 [14].

$$A(\omega) = \frac{F_0/m}{\left[(\omega_0^2 - \omega^2)^2 + (\omega\omega_0/Q)^2\right]^{1/2}} \qquad (2.5)$$

The oscillation amplitude of the cantilever is kept constant at a set point, where the distance between the tip and the surface is therefore adjusted by a piezotube using a controlled feedback mechanism. Thus, the modulation of the amplitude due to the interaction between the tip and the surface, given by the equation is used to extract the topography. Van der Waals, electrostatic forces and magnetic forces are attractive forces and can be more dominant in dynamic (tapping, non-contact) modes.

Similar to tapping mode, in non-contact mode AFM, the cantilever is excited to oscillate at with a specific amplitude at its resonance frequency. Depending on the interaction forces between the tip and the surface, F_{ts}, the resonance frequency (ω_0) of the cantilever is shifted and this is called the new effective resonance frequency (ω_{eff}) . The frequency shift is approximated as in equation 2.6 [14].

$$\Delta\omega = \omega_{eff} - \omega_0 \approx - (\omega_0 k_{ts}/2k) \qquad (2.6)$$

Here, k and k_{ts} are cantilever stiffness and tip-surface interaction stiffness, respectively. When the cantilever and the tip-surface interaction are considered as a one total system with an effective spring constant k_{eff}, the new effective resonance frequency, ω_{eff} can be extracted with equation 2.7.

$$\omega_{eff} = \left(k_{eff}/m\right)^{1/2} \qquad (2.7)$$

Where the effective spring constant k_{eff} is given by equation 2.8.

$$k_{eff} = k - k_{ts} \qquad (2.8)$$

The frequency shift depends on the interaction regime, where attractive forces lead to a decrease of the resonance frequency, repulsive forces result in an increase in the resonance frequency, as shown in Figure 2.5 [14].
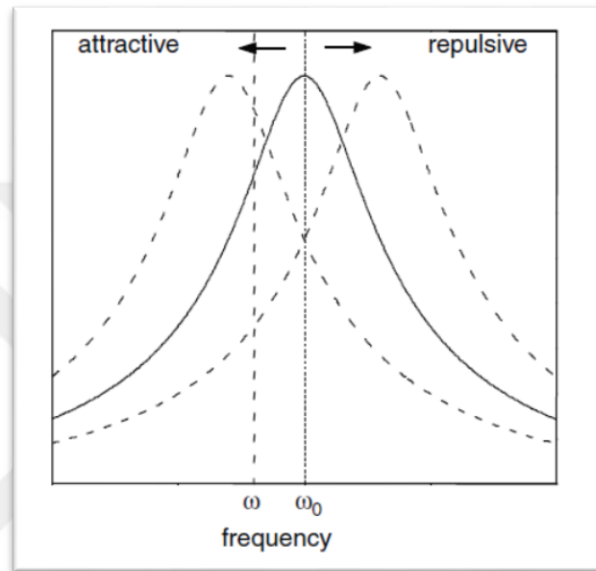
Figure 2.5 : The shift of resonance frequency depending on the interaction regime [14].

Keeping this frequency shift constant by using a feedback loop, the surface is scanned in x and y directions.

2.2 Simultaneous STM/AFM

Considering the capability to measure the different characteristics of a surface at the same time, obtaining simultaneous STM and AFM information by different channels enables further investigations in scanning probe microscopy. In the last few decades, there have been two main systems developed with the aim of conducting STM and AFM simultaneously on the surfaces. Operating the STM and AFM simultaneously is possible using typical AFM setups. However, the true simultaneous operation of the STM and AFM requires smaller oscillation amplitudes. This is either achieved by

using very sensitive deflection detection methods as in the system used in this work, or as an alternative, with the use of the tuning fork.

In the system based on the tuning fork, which is developed by Giessibl in 1998, a quartz crystal resonator with a specific resonance frequency is used [16]. The operation is based on the method of frequency modulation mode AFM, where the frequency shift is used as the feedback while the tuning fork is oscillated at resonance frequency. Additionally, the tunneling current between the tip implemented on the tuning fork and the surface is recorded simultaneously.

One of the other main simultaneous STM/AFM systems, which is also used in this study, is mainly utilized by the fiber-optic interferometer setup as a deflection detection sensor [17]. In this system, the tunneling current is used as a feedback, while the cantilever is oscillated at frequencies well below its resonance. This enables the true measurement of the tunneling current, since the cantilever oscillations are at sub-Ångström level. The topography is obtained by using the tunneling current feedback. Besides, using two different lock-in amplifiers, the cantilever oscillation amplitude, phase shift and the tunnel current modulation at the oscillation frequency of the cantilever are recorded as three separate channels. While scanning, the deflection of the cantilever due to the interaction between the tip and the surface is also recorded as a separate channel using the fiber-optic interferometer setup, which will be discussed further in the next section.

The setup consists of a modified STM/AFM head shown in Figure 2.6, implemented into a commercial OMICRON system. The modification also includes a fiber-optic interferometer setup designed to detect the cantilever deflection. The STM/AFM head is located on a plate and the vibration isolation is maintained by springs and additionally by Eddy-current dampers. The STM/AFM is controlled by the software and electronic unit by NanoMagnetics Instruments.
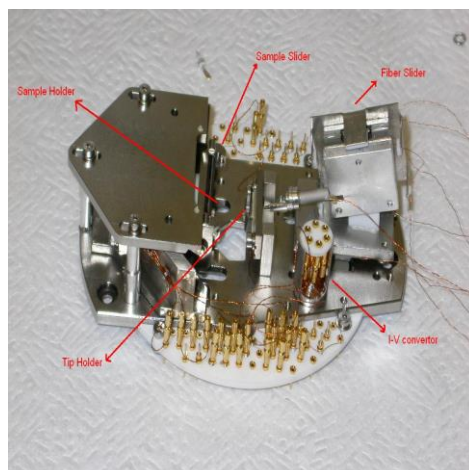
Figure 2.6 : Home-built simultaneous STM/AFM head.

The whole unit is installed in a commercial OMICRON ultra-high-vacuum chamber shown in Figure 2.7, with a base pressure of $2x10^{-10}$. This pressure is achieved with the use of four different pumps, which are a turbomolecular pump supported with a mechanical rotary pump, ion-getter pump and a titanium sublimation pump.

Figure 2.7 : UHV system.

Additionally, this system is equipped with an ion-sputter gun and a manipulator that has resistive-heating and direct-current heating units, for annealing the samples at different temperatures.

2.2.1 Fiber-optic interferometer setup

Determining the cantilever oscillation amplitude at sub-Ångström level is enabled with the use of fiber-optic interferometer setup. The fiber-optic interferometer setup used in this study is utilized by a laser diode coupled into a single mode 2x2 fiber splitter. The fiber is fed with one of the outputs of the fiber splitter and is placed located at the closest position to the back of the cantilever. Moreover, fiber is attached to a five-axis positioner built with shear piezos, as the alignment of the fiber in x, y, z, θ and φ is achieved by this positioner. The other output of the splitter is given to the reference photodiode, where the input of the splitter is given to the signal photodiode. The mechanism of this setup is presented in Figure 2.8, is based on the Fabry-Perot interferometer [18], as a small cavity between the fiber and back of the cantilever is maintained. The beam of light travelling through the fiber is reflected from the end of the fiber and the rest travelling through the end of the fiber is reflected from the back of the cantilever, returns to the fiber. In the small cavityformed, the interference of these two beams results in a photocurrent at the signal photodiode. The reference photodiode is used to eliminate the probable noise and power fluctuations, as it is subtracted from the signal photodiode.
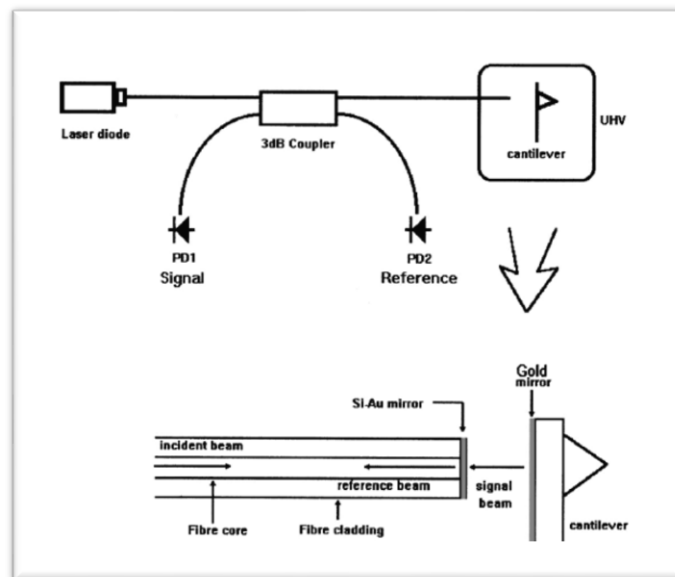
Figure 2.8 : Schematics of all-fiber interferometer setup [17].

With the use of the photocurrent detected on the signal photodiode, an interference pattern is formed, as in Figure 2.9. When the fiber is aligned properly, the slope of this interference pattern is given by equation 2.9.

$$\Delta i / \Delta d = 4\pi i_0 V m / \lambda \qquad (2.9)$$

where i, d, V and λ are signal photodiode current, distance between cantilever and the fiber, visibility and laser wavelength, respectively. This is converted to sensitivity in Ångström/volts.
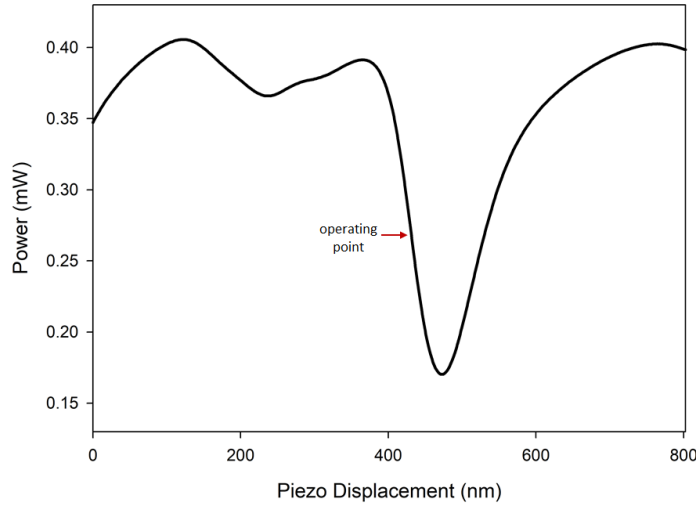
Figure 2.9 : Typical interference pattern. Operating point is indicated by red arrow. This point is the most sensitive point for this particular interference pattern, with the maximum slope (-181.98 mV/Å).

Before scanning the surface, the fiber is aligned by a piezotube at the most sensitive position, quadrature point, on the interference pattern. The slope of the pattern at this point is measured and this allows calculation of the oscillation amplitude and deflection of the cantilever in units of Ångström.

2.2.2 Cantilever calibration

One of the main elements of the Atomic Force Microscopy is the cantilever, in order to obtain atomic resolution but also to extract the mechanical properties of the surface as well. Since the quantitative measurement of the force is significantly related on being acquainted with the characteristics of the cantilever, calibrating the cantilever carefully is essential. As discussed in the previous sections, the resonance frequency and the stiffness are the most important mechanical properties of the cantilever and therefore need to be considered in more detail.

The cantilever resonance frequency is given as a function of the dimensions of the cantilever, density and the Young's modulus as in equation 2.10.

$$\omega^2 = \frac{0.314EI}{L^4\rho S} \tag{2.10}$$

The cantilever stiffness k is expressed as below,

$$k = \frac{3EI}{L^3} \tag{2.11}$$

The equation 2.11 is a primitive method to obtain a value for stiffness roughly. Thus, various calibration techniques have been developed, in order to calibrate the cantilevers more precisely. For this study, the extraction of the cantilever stiffness k is achieved by using the thermal noise method, where the equipartition theorem leads to the relation of the thermal energy of the cantilever and its stiffness by equation 2.12.

$$\frac{1}{2}k\langle z^2 \rangle = \frac{1}{2}k_B T \tag{2.12}$$

In the calibration method suggested by Fukuma [19], the thermal Brownian noise curve of the cantilever which is plotted by using equation 2.13 is fit to the measured thermal resonance curve. This is accomplished by setting reasonable values for the Q factor and the cantilever stiffness k, in equation 2.13, where k_B and T are the Boltzmann's constant and the absolute temperature, respectively.

$$n_{zB} = \sqrt{\frac{2k_B T}{\pi \omega_0 kQ} \frac{1}{\left[1-(\omega/\omega_0)^2\right]^2 + [\omega/(\omega_0 Q)]^2}} \tag{2.13}$$

For the particular highly boron doped diamond cantilever, k is approximately obtained as 70 N/m, by fitting of the Brownian noise curve on the thermal resonance curve acquired by the lock-in amplifier, as shown in Figure 2.10.
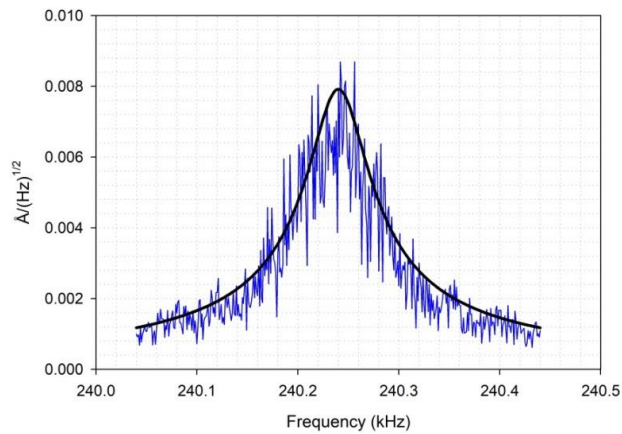
Figure 2.10 : Fit of the Brownian noise of the highly boron doped diamond cantilever on the thermal resonance curve, by approximating the stiffness $k \approx 70$ N/m.

2.2.3 Quantities measured using simultaneous STM/AFM

As in every STM, in simultaneous STM/AFM, the electronic characteristics of a surface are revealed based on the measurement of the tunneling current between the tip and the surface. In the simultaneous STM/AFM system used in this study, the surface topography is obtained by using the tunneling current as a feedback. In addition to that, the main advantage of simultaneous STM/AFM is obtaining the mechanical characteristics of the surface related to force interaction between the tip and the surface at the same time. The cantilever is oscillated at a specific off-resonance frequency, which leads to small (sub-Ångström) oscillation amplitudes. This brings the opportunity to make sure that the set tunneling current is not largely manipulated by the oscillations and therefore the operation regime is always determined. The excitation of the cantilever is maintained by using a lock-in amplifier and the oscillation amplitude signal is measured through the same lock-in, in volts. Before the cantilever is approached to the surface, out of the interaction, the free oscillation amplitude A_0, is recorded. As the cantilever is approached to the surface, the oscillation amplitude changes due to force interaction. Therefore, the interaction stiffness k_{int}, between the surface and the tip is extracted as a function of the cantilever stiffness k_0, free oscillation amplitude A_0 and the oscillation amplitude in interaction A, with the use of the formula given by equation 2.14.

$$\frac{dF}{dz} = -k_{int} = k_0 \left(1 - \frac{A_0}{A}\right) \tag{2.14}$$

When the cantilever is excited, a phase shift occurs between the excitation signal and the cantilever oscillation. With the use of the lock-in amplifier, this phase shift is measured. Once the cantilever is approached to the surface, this phase shift changes due to interaction and can be recorded at each point, during the scan. Measure of the phase shift may reveal the energy dissipation with a good approximation as given in equation 2.15 [20].

$$E_{loss} = \frac{2\pi P_{int}}{\omega} = \frac{\pi}{4} k_0 A_0 A sin\varphi \tag{2.15}$$

where P_{int} and ω are the power dissipated by the interaction between the tip and the surface and the oscillation frequency, respectively.

The excitation frequency of the cantilever oscillation, which is determined on the main lock-in amplifier is fed to another lock-in amplifier as reference frequency, in

18

order to measure the variations on the oscillation of tunneling current. The small oscillations around the set tunneling current at the cantilever oscillation frequency are measured using this lock-in amplifier. Tunneling current modulation is one of the important quantities that could be measured by this system, as it allows the determination of the barrier height at each point of the scanned surface. The barrier height ϕ is obtained by the formula given by Lang [21] in equation 2.16.

$$\phi = 0.95 \left(\frac{dlnI}{dz}\right)^2 = 0.95 \left(\frac{1}{I}\frac{dI}{dz}\right)^2 \qquad (2.16)$$

Moreover, surface electronic properties, which are mainly based on the local density of states, can be evaluated further by *I-V* spectroscopy. The *I-V* spectroscopy is achieved by measuring the dependence of the tunneling current on the applied bias voltage.

2.2.4 Force-distance spectroscopy

Mostly, the main aim of the AFM studies so far has been to obtain information related to the surface, arising from the force interaction between the cantilever and the surface. Starting from this point of view, the quantitative measurement of this interaction force is a key point to shed light on the surface characteristics. In the system used in this study, by changing the distance between the tip and the sample, it is possible to measure the force, interaction stiffness, tunnel current modulation (barrier height), phase shift (energy dissipation) and tunneling current simultaneously. At a specific point on the surface, the sample is retracted to a point out of the interaction regime and then approached to the tip, until it reaches the desired set tunnel current limit.

All the quantities mentioned above are recorded, and can be evaluated as a function of the tip-surface distance. Conduction force-distance spectroscopy at different points on the surface using different parameters helps to reveal the mechanical and electronic characteristics of a surface or even of a specific atom on the surface. In this study, a tungsten (W) cantilever and a highly boron doped diamond cantilever are used to conduct force-distance spectroscopies, as well as to scan the surfaces.

3. DIAMOND SURFACE

3.1 Types and Characteristics of Diamond

Diamond is one of the carbon-based materials that naturally exist. It is an allotrope of carbon, which has a diamond cubic lattice structure, as displayed in Figure 3.1, with a lattice constant of 3.57 Å, consisting of tetrahedrally bonded carbon atoms, with two carbon atoms per primitive unit cell. Since its discovery, it has always been a precious rock for cultures, as it is a rarely found material. Besides being a gemstone, diamond has several characteristic properties, which separates it from any other material. Diamond has its reputation due to its physical hardness and high thermal conductivity. The rigidity of the diamond originates from the strong covalent bonds between the carbon atoms, which makes it to be the hardest material on Mohs scale. The bulk modulus of the diamond is given as 4.4×10^{11} N/m^2, which makes it impossible to be scratched by any other material, but only by diamond itself [22].
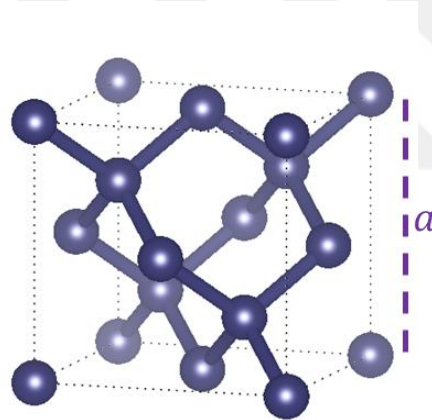
Figure 3.1 : Diamond lattice structure, the lattice constant a=3.57 Å.

The existence of diamond in the nature might be in various types, depending on the impurities it contains. These impurities are mostly boron or nitrogen, since the reactivity of the strong lattice structure only allows for some materials to be contaminated. The impurities or defects are identified by the colour of diamond, such as boron impurities convert the colour of the diamond to blue, where nitrogen impurities convert its colour to yellow. Moreover, the impurities may also change the hardness and electronic characteristics of the diamond. It is known that boron impurities lead to the semiconductivity of diamond, whereas naturally diamond is insulator with a bandgap of 5.47 eV [23]. Diamond is mainly classified in two types

as Type I and Type II, depending on the amount of nitrogen impurity it contains. Type I and Type II are also divided into two as Type Ia, Type Ib and Type IIa, Type IIb respectively. The mostly found diamonds in nature are Type Ia. They show a higher concentration of nitrogen with respect to the other diamond types. Type II diamonds do not contain much of a nitrogen impurity. Where Type IIa diamonds have the highest thermal conductivity among all other diamond types, Type IIb diamonds can include boron impurities, which leads them to show p-type semiconductor properties.

This diversity of the properties of diamonds opened up the way for the usage of different types of diamond in various fields. Therefore, the synthesis of diamond as thin films, or as bulk, poly/single crystalline surfaces, with different methods has been focused on. The growth of diamond has been achieved by high pressure/high temperature and CVD methods [24]. CVD growth process is primarily performed with the use of methane, as the carbon source gas and atomic hydrogen, as the etching component for the graphitic phases and as the surface stabilizer.

3.2 Cleaning the Diamond Surface

For the investigation of surfaces at the atomic level, it is essential to obtain topologically flat and atomically clean surfaces. This requires different techniques and parameters depending on the surface properties. Diamond is a material well known with its hardness regarding the surface structure due to its sp^3 bonds. Cleaning the diamond surface in an atomic level is challenging, considering the possibility of the graphitization of the diamond through breaking the sp^3 bonds in to sp^2 bonds. Different methods such as sputtering, annealing, acid-etch and Hydrogen plasma etch are used in order to clean the diamond surface [25]. Hydrogen plasma is commonly used during the growth process of diamond in CVD, since atomic hydrogen etches the graphitic phases on the diamond surface and makes it possible to obtain a stable diamond phase [4]. Acid-etch is another common method for the chemical cleaning of the diamond surface. Various kinds of acids and their combinations are used to remove the graphitic material, metallic impurities and other contaminants due to the exposure of diamond surface to air [26]. Furthermore, one of the most studied surface cleaning techniques is sputtering, to remove the contaminants off the surface and typically annealing the surface afterwards.

3.2.1 Sputtering

Sputtering is one of the common methods used to clean the surfaces, in most of the STM/AFM studies in UHV. Sputtering is the heavy ion bombardment of the surface resulting in the removal of the layers from the surface, leaving the surface clean and pure without any undesired material. Argon gas is used for the sputtering of the surfaces, since the reactivity of the Argon with the surfaces is limited due to its noble gas properties. In the system used in this study, OMICRON ISE 5 ION SOURCE, the Argon gas is let into the chamber using a leak valve. The target current is obtained with the ionization of the Argon, which is enabled by the potential difference between the cathode (gas cell) and anode. Thus, beam energy and target current can be adjusted, with the generated ions and electrons, respectively. Moreover, the beam is focused to the sample surface using a focus element.

Sputtering of the diamond is a highly studied method, mostly because it enables the graphitization of diamond. This is possible by damaging the surface by breaking the sp^3 bonds in to sp^2 bonds using high beam energies, exceeding a threshold value of defect density, e.g. $1x10^{22}$ vacancy/cm^3 [27]. This threshold value may be unique for each sample, since the dopants and natural defects could be different from sample to sample [28]. In this study, mainly *gentle* sputtering is used to obtain a clean diamond surface. This is achieved by trial of different beam energy values, 0.5 keV and 1 keV, and durations. Considering the damage occuring on the surface during sputtering, in order to observe the effect of minimization of the damage, different angular orientations, 30, 60 and 90 degrees, of the ion bombardment are also tried. Besides, graphitization of diamond is also studied, using longer sputtering durations.

3.2.2 Annealing

Following the sputtering process, it is generally required to anneal the surfaces to different temperatures depending on the material properties, in order to obtain an atomically flat and smoother surface, healing the damage caused by sputtering. The annealing unit used in this study is shown in Figure 3.2, provides two different mechanisms for annealing. These are resistive heating and direct current heating. Both techniques are applied by placing the sample on the manipulator, which is designed with the heating elements. Resistive heating enables heating the samples up

to 800-900°C, by using a tungsten filament. This is achieved by passing current through the tungsten filament attached to the sample manipulator, increasing the current leads to increase in the filament's temperature and therefore the sample is heated. Another method for heating the samples is direct current method. This is conducted by passing current through the silicon sample mounted tightly under the sample.
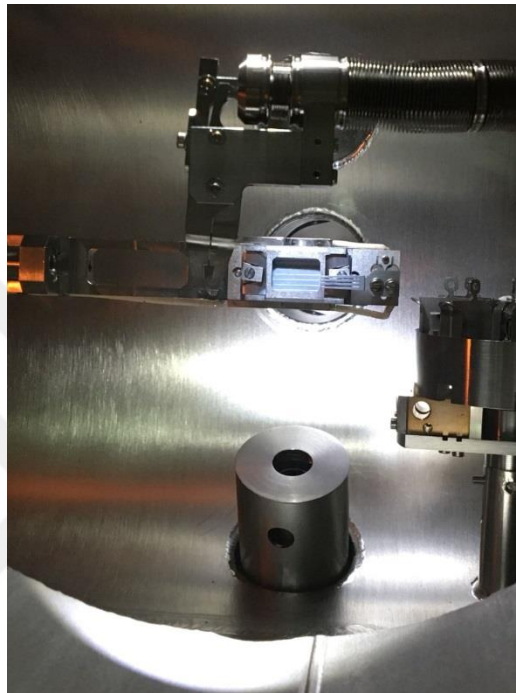
Figure 3.2 : Sample manipulator and sputter gun from inside of the UHV chamber.

In our system, controlling the voltage and current parameters, it is possible to reach temperatures up to 1100°C. In order to examine the effect of annealing at different temperatures on the cleaning process of diamond, both techniques are used in this study. Annealing temperatures may differ for each material, regarding the phase transitions of the material. In the case of diamond, several critical temperature values were determined. The removal of typical contaminants such as H_2O, O_2, CO_2, or CH_3, due to the exposure of the diamond to ambient conditions, is achieved by annealing the diamond sample to 450-650°C. Since the CVD grown diamonds mostly contain hydrogen or they are intentionally hydrogen terminated or hydrogenated, in order to dehydrogenate the diamond and to observe the clean diamond surface, annealing the surface at around 1000°C is required. Similarly, to get rid of the oxidation, which mostly results from the acid-etch; it is necessary to anneal the surface to temperatures around 900-1050°C [29]. An important annealing

temperature is the point where the phase transition from diamond to graphite occurs. It is known that the graphitization occurs at temperatures higher than 1300°C [30].
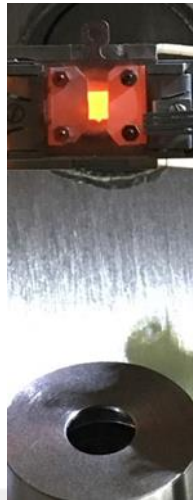
Figure 3.3 : Image of the sample on the sample manipulator during the heating process.

3.2.3 Acid etch

Diamond's rigid physical structure makes it possible to use chemical acids in order to clean the surface. Even the strongest acids are known to be safe to use on diamond, as they give no harm to the diamond itself. Thus, in most of the scanning probe microscopy studies on diamond, acid etch is a preferred technique to remove the probable contaminants off the surface. The types of acids and mixtures are chosen by targeting the kinds of contaminants existing on the diamond surface. During the CVD growth process of diamond, formation of graphitic phases is common. In order to remove these graphitic phases, chromic acid is used. Similar non-diamond impurities originating from the growth process may also be removed by using a warm solution of 30% H_2O_2 [31]. Besides, metallic contaminants may exist on the surface, originating from the substrates used in the growth process. Aqua regia ($3HCl:1HNO_3$) is often used to eliminate the metallic contamination from the surface [32].

Even though acid etch has been one of the most effective methods to obtain cleaner diamond surfaces, it has several disadvantages. One of the main reasons that acid etch is not considered to be safe is that working with these acids may be hazardous, as they mostly contain strong chemicals, and therefore requires much more attention.

Additionally, using these acids on the diamond surface leaves the surface highly oxidized. Even though it is possible to remove the oxidation by annealing the surface at specific temperatures, excessive oxidation might require longer durations of annealing, which may result into degradations on the diamond surface structure.

In this study, the acid etch procedure was conducted as boiling in each acid respectively and distilled water rinse after each one. Firstly, the samples were kept in boiling saturated chromic acid for 10 minutes, in order to remove the probable graphitic impurities on the surface and they were rinsed in distilled water subsequently. After that, the samples were waited in hot aqua regia for 30 minutes with the aim of eliminating the probable metallic contaminants on the surface, and this was followed by distilled water rinse. For all other non-diamond impurities that might have been formed on the surface, the samples were placed in warm solution of 30% H_2O_2 for 30 minutes and finally the samples were rinsed in distilled water. This was followed by a typical chemical cleaning procedure for UHV, which consists of consequent rinse in acetone, isopropanol and distilled water, separately.

4. RESULTS

In this section, the results will be given on the ambient AFM and simultaneous STM/AFM imaging of the two different polycrystalline diamond samples and single crystalline diamond surfaces. Both surfaces are prepared using different sputtering and annealing parameters, and also acid etch. Various scan parameters are used while scanning the surfaces. Force-distance spectroscopies are also performed on multiple points on each surface, using different bias voltage values.

4.1 Polycrystalline Diamond Surfaces

The polycrystalline diamond sample studied by AFM in ambient conditions is a CVD grown sample on silicon substrate. The sample was scanned in tapping mode, using commercial Si cantilever with approximated stiffness of 40 N/m. The sample is known to be unpolished, and the cubo-octahedral growth of the diamond structures could be observed in AFM images given in Figure 4.1. Surfaces with different growth orientations of the diamond are observed.
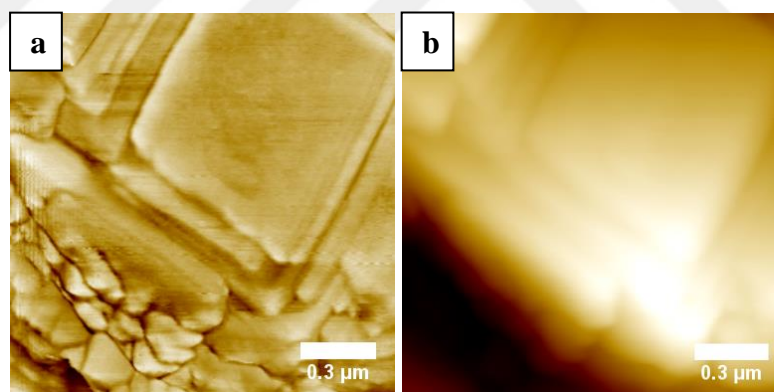
Figure 4.1 : Tapping mode AFM images of the polycrystalline diamond surface grown on Si substrate (a) phase shift (b) topography.

Large area scan of the same polycrystalline diamond sample by AFM in ambient conditions is given in Figure 4.2. Similar to the small area scan, cubo-octahedral diamond structures are easily seen, revealing a variety of different growth orientations.
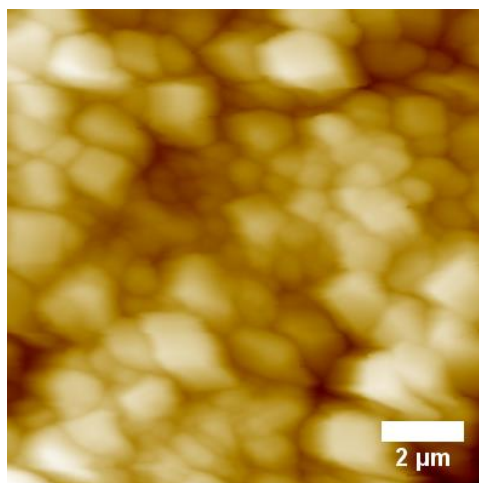
Figure 4.2 : Tapping mode AFM topography image of the polycrystalline diamond surface grown on Si substrate.

The polycrystalline diamond surface studied by simultaneous STM/AFM in this work was grown on a molybdenum substrate, by CVD. Even though the exact dose is unknown, the sample is modestly doped with nitrogen. Furthermore, after the growth process, the sample was polished using diamond grits. Different samples of the same polycrystalline diamond surface were prepared in order to investigate various cleaning techniques. Subsequently, each sample was studied by simultaneous STM/AFM, which the results will be discussed in the following. The optical microscopy image of the polycrystalline sample surface is given in Figure 4.3.
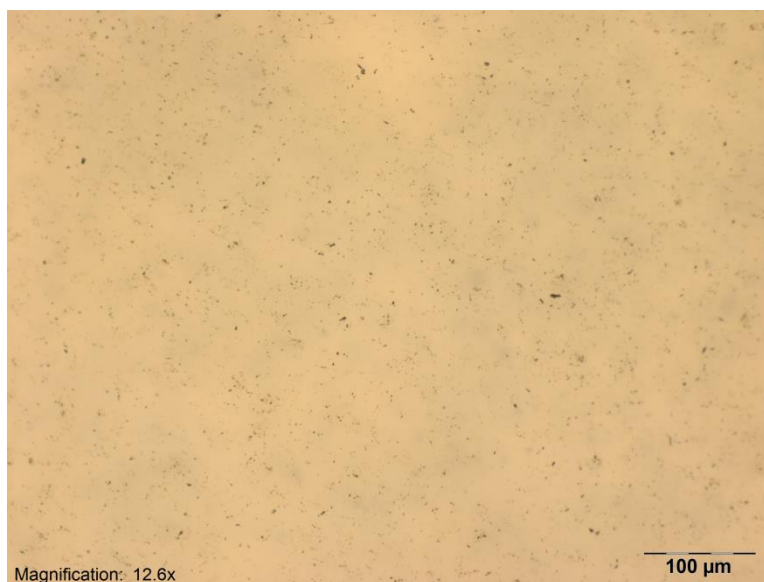
Figure 4.3 : Optical microscopy image of polished polycrystalline diamond surface grown by CVD.

After the typical cleaning process of the sample in acetone, isopropanol and distilled water subsequently, the sample was placed to the UHV chamber. Firstly, in order to

28

check whether the tunnel current could be obtained without any further cleaning process, the sample was only annealed at 800°C. However, tunnel current was not acquired. This was followed by a sputtering with 1 keV beam energy for 15 minutes and an anneal at 800°C for 15 minutes after that. This enabled to obtain tunnel current and the surface was scanned by simultaneous STM/AFM.

In this work, both large and small area imaging of polycrystalline diamond surfaces are achieved. The initial large area scans of the surface were mainly studied in STM mode. The resulting large area scans show the polish lines in STM topography images, as seen in Figure 4.4.
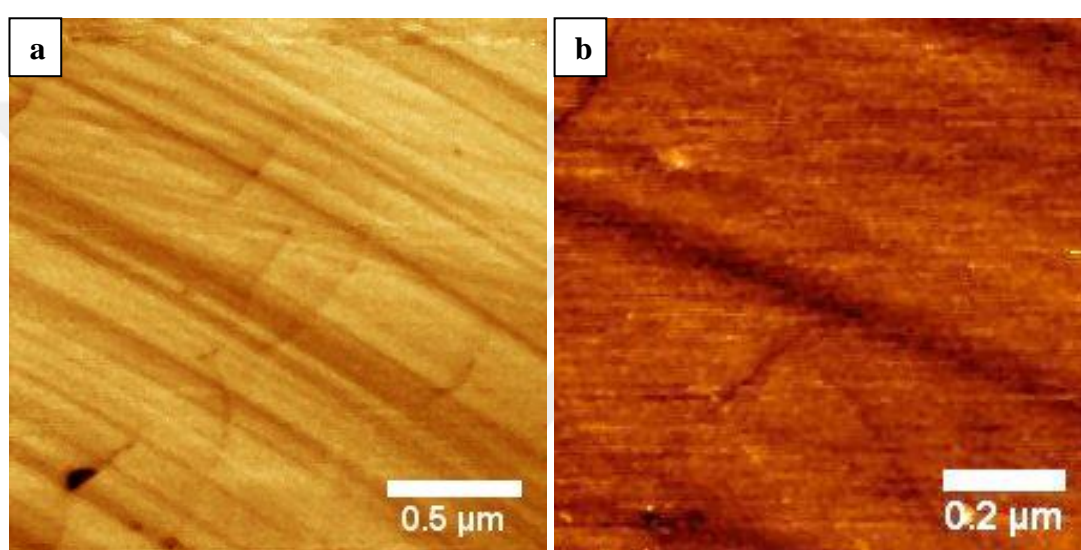
Figure 4.4 : UHV STM topography images of the polycrystalline diamond surface with the set parameters (a) V_{bias}: 6 V. I_t: 0.25 nA (b) V_{bias}: 5.5 V. I_t: 0.55 nA.

In addition, Figure 4.5 shows the smaller area STM topography in the same region shows a granular structure, which could be interpreted as an amorphous layer of carbon. This amorphous layer of carbon could be revealing the graphitic phases on the surface. Consequently, for the removal of the probable contaminations such as graphitic or metallic, the acid etch was considered as an alternative chemical cleaning procedure.
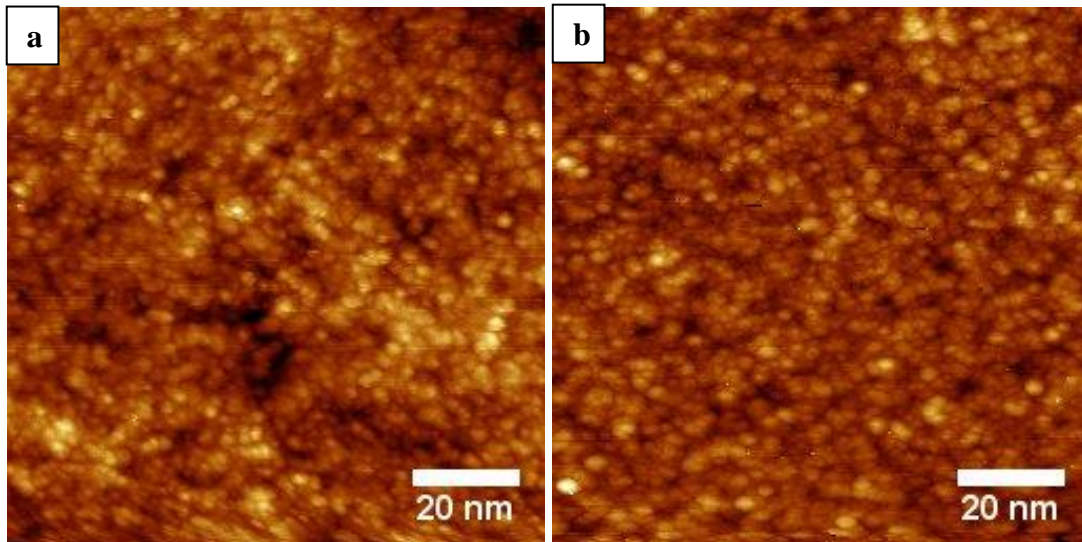
Figure 4.5 : UHV STM topography images of the polycrystalline diamond surface obtained by using W lever, with the set parameters (a) V_{bias}: 4 V. I_t: 0.35 nA (b) V_{bias}: 2 V. I_t: 0.35 nA.

After the acid etch was performed on this polycrystalline diamond sample, the typical chemical cleaning routine was repeated by using acetone, isopropanol and distilled water. The diamond sample was introduced to the UHV chamber and it was annealed by direct current heating at 950°C for 15 minutes, in order to remove the oxide layer, resulted from the acid etch. After annealing, no tunneling current was observed. It was considered that the duration of the anneal was not sufficient for the removal of the excessive amount of oxidation. As discussed in the previous chapter, since the longer durations of annealing in high temperature might cause damaging, a gentle sputtering using 0.5 keV beam energy for 10 minutes, with sample plane oriented at 30° angle with respect to the sputter gun was performed. After sputtering and subsequent annealing, tunnel current was obtained and the surface was scanned in simultaneous STM/AFM mode. In Figure 4.6, large and smaller area scans of the surface show an ordered structure compared to the previous results. This could imply that the controlled gentle sputtering is an efficient procedure for the cleaning of the diamond surface.
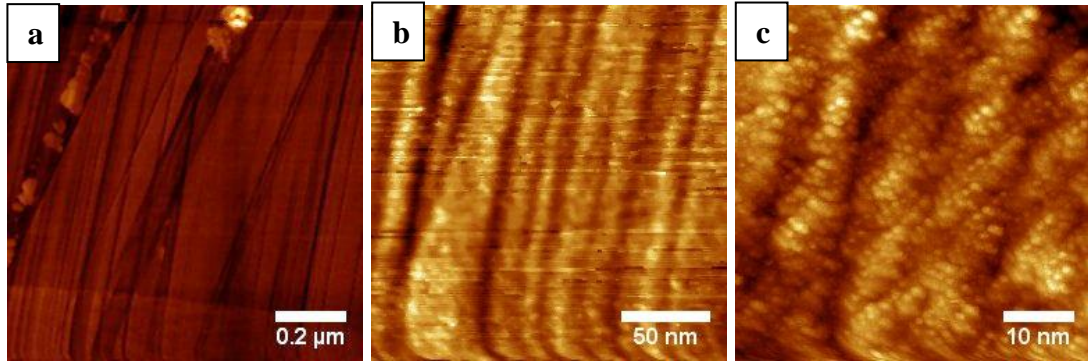
Figure 4.6 : UHV STM topography images of the polycrystalline diamond surface obtained by using W lever, with the set parameters (a) V_{bias}: 8 V. I_t: 0.3 nA (b) V_{bias}: 8 V. I_t: 0.3 nA (c) V_{bias}: -1 V. I_t: 0.3 nA.

Results of simultaneous STM/AFM imaging of a 500 $Å^2$ scan area on the same sample, using highly boron doped diamond cantilever are shown in Figure 4.7, including tunnel current modulation (measure of barrier height), inverted oscillation amplitude (measure of interaction stiffness), phase shift (measure of energy dissipation) and STM topography channels. In this scale of imaging, an ordered construction of the surface is not observed. This may be due to the inhomogeneous surface cleaning.
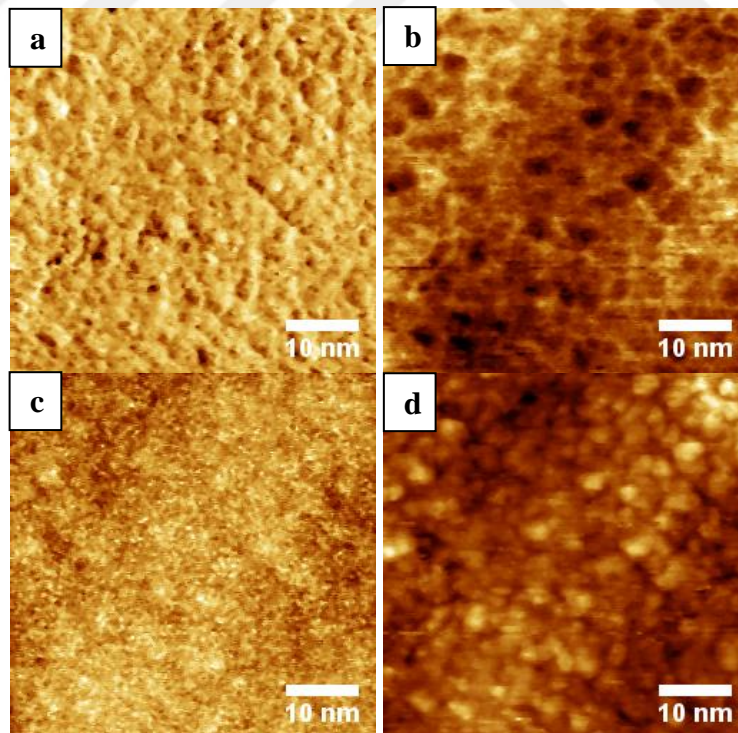
Figure 4.7 : UHV simultaneous STM/AFM images of the polycrystalline diamond surface obtained by using highly doped diamond cantilever, with the set parameters V_{bias}: 3 V. I_t: 0.3 nA $A_0 = 1$ $Å_{(p-p)}$ $f_0 =240430$ Hz f=27484 Hz (a) tunnel current modulation (b) interaction stiffness (c) phase shift (d) STM topography.

As discussed before, ion bombardment with high energies and long durations may result a phase change from diamond to graphite, in the condition of exceeding the value of defect density threshold [28]. One of the samples prepared from the same polycrystalline diamond surface was focused on with the attempt to obtain graphite layers. Thus, the sample was sputtered using 1 keV beam energy for 1.5 hours and subsequently annealed at 800°C. After a while the sample was annealed at 400°C and then studied by simultaneous STM/AFM. Below, the STM topography images of the sample after this process are given in Figure 4.8. The hexagonal structures occurred on the surface are supposed to indicate the formation of graphitic islands. These hexagonal islands have a dimension of approximately 0.5 μm. In fact, considering the possibility of multiple tip imaging, the existence of such hexagonal structures on the surface is a certain sign of creation of potential graphitic phases.
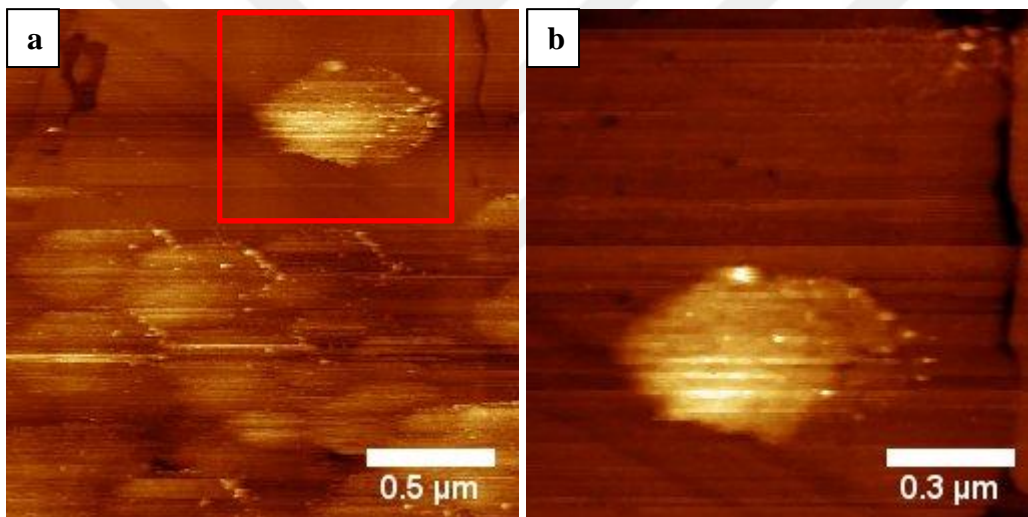

Figure 4.8 : UHV STM topography images of the polycrystalline diamond surface obtained by using W tip with the set parameters (a) V_{bias}: 7.5 V I_t: 0.25 nA (b) V_{bias}: 8 V I_t: 0.25 nA.

4.1.1 Different domains

While scanning the polycrystalline surfaces, it is expected to observe different domains and crystallographic orientations, since the growth of the sample is not in a specific orientation. In several regions on the surface, domain-like structures were observed, as seen in Figure 4.9 (a) and Figure 4.9 (b). In Figure 4.9 (a), four different regions can be seen. This is interpreted as the difference in brightness of these regions is not due to the height changes but due to the variation of the electronic characteristics. It is supposed that obtaining tunnel current in specific domains might

be easier with respect to the others. This is expected since the conductivity of surface is affected by the crystallographic orientation [33]. Similarly, in Figure 4.9 (b), two different regions are revealed. It is seen that the form of minor structures change through the diagonal border.

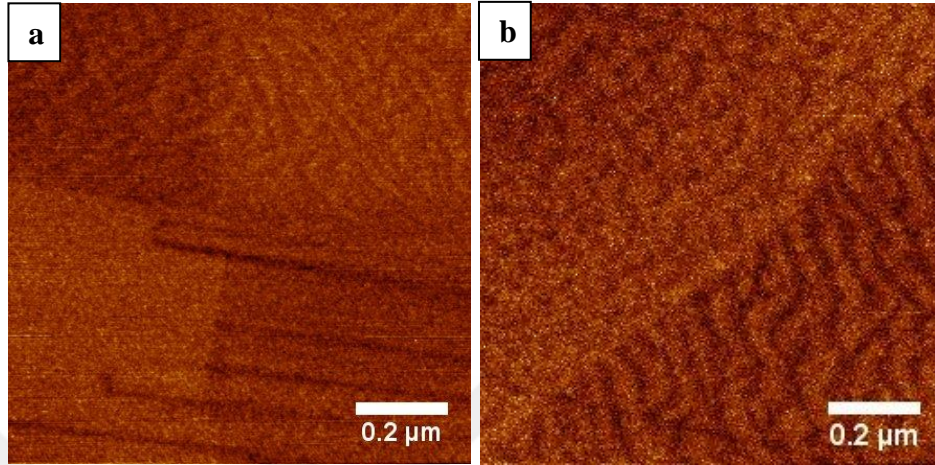

Figure 4.9 : UHV STM topography images of the polycrystalline diamond surface with the set parameters (a) V_{bias}: 8 V I_t: 0.2 nA (b) V_{bias}: 8.5 V I_t: 0.22 nA.

In Figure 4.10, different regions were observed, in both STM topography and force gradient images. The horizontal darker lines seen in both images are supposed to be the polish marks. It is possible to see the forms of the structures differ in the diagonal fragment and the rest of the scan. In the upper right section of the STM topography, two different arrangements can be noticed. The change in the brightness of this part may be due to the surface topography, or due to the difference in electronic properties of these two differently arranged regions, as mentioned in the previously.
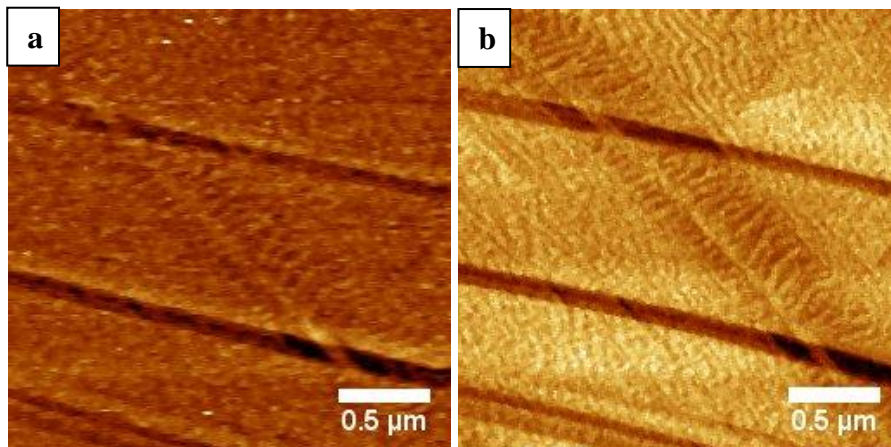
Figure 4.10 : UHV simultaneous STM/AFM images of the polycrystalline diamond surface obtained by using W cantilever, with the set parameters V_{bias}: 4 V. I_t: 0.2 nA $A_0 = 0.8$ Å$_{(p-p)}$ f_0 =31512 Hz f =15380 Hz (a) interaction stiffness (b) STM topography.

4.1.2 Atomic resolution imaging

The polycrystalline diamond was studied further with the aim of imaging the surface in atomic scale. As mentioned previously, the polycrystalline surfaces are rich in crystallographic orientation. Therefore, it was expected to observe different crystallographic structures and to investigate their electronic and mechanical properties as well.

The initial atomic resolution results are presented in Figure 4.11. The tunnel current modulation (measure of barrier height), inverted oscillation amplitude (measure of interaction stiffness) and the STM topography are demonstrated. As expected, the regions with different crystallographic structures are detected obviously even in this scale. Even though the periodic structures are mostly observed, the surface also seems to contain amorphous regions partially.
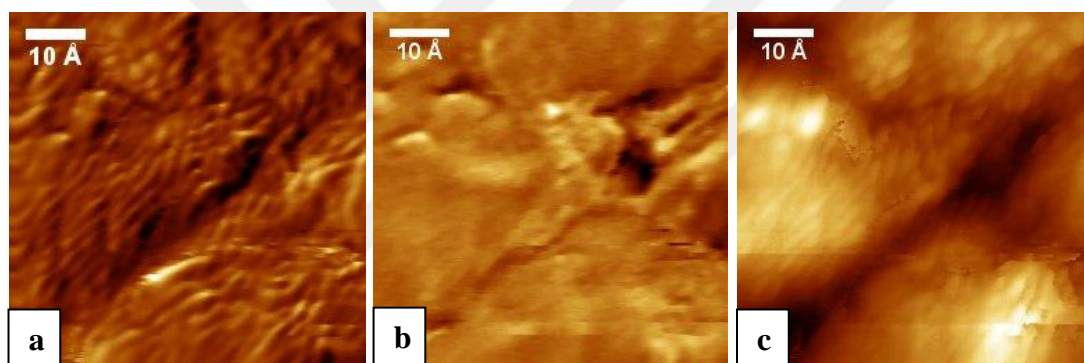

Figure 4.11 : UHV simultaneous STM/AFM images of the polycrystalline diamond surface obtained by using W cantilever, with the set parameters V_{bias}: -500 mV. I_t: 0.35 nA $A_0 = 0.6$ Å$_{(p-p)}$ $f_0 = 31512$ Hz f $= 19834$ Hz (a) tunnel current modulation (b) interaction stiffness (c) STM topography.

Below, another atomic resolution image of the same polycrystalline surface is represented in Figure 4.12. A tungsten (W) lever with stiffness of k=53 N/m was used to scan the surface. These results were obtained using comparatively lower values of bias voltages, such as -700 mV. There is a specific crystallographic structure in the marked region, also seen in zoomed as well. This structure shows considerable similarity to the previously reported (111) oriented surface [7]. Moreover, this region was studied in more detail, by calculation of the interaction stiffness and the barrier height as well. In this zoomed region of estimated (111) structure, the barrier height range is between 0.02 eV and 4.83 eV, as shown in Figure 4.12 (a). The range of barrier height values are considerable compared to the

previous works [26]. As previously mentioned, the surface electronic characteristics vary due to the crystallographic orientation, dopants, surface cleaning and surface termination.

The interaction stiffness for the same region was also calculated, as shown in Figure 4.12 (b). The values for interaction stiffness are in the range of -14 N/m to 10 N/m. The relation between the interaction stiffness (force gradient) and the force enables to specify the interaction regime. The positive values for interaction stiffness indicate the repulsive regime, where the negative values imply attractive regime of force.

The STM topography is given in Figure 4.12 (c). All three images of the same region are in a good agreement, when compared. Being able to scan the surface with such low bias voltage may suggest that the surface is not highly oxidized or contaminated.
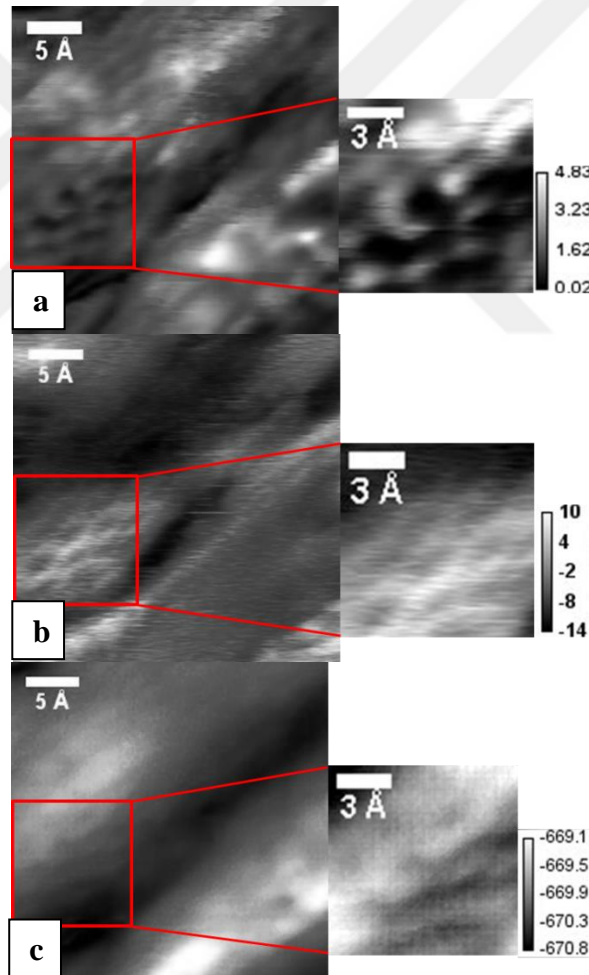
Figure 4.12 : UHV simultaneous STM/AFM images of the polycrystalline diamond surface obtained by using W cantilever, with the set parameters V_{bias}: -700 mV. I_t: 0.55 nA $A_0 = 0.6$ Å $_{(p-p)}$ $f_0 = 31512$ Hz $f = 19834$ Hz (a) tunnel current modulation and barrier height of marked region (b) interaction stiffness (c) STM topography.
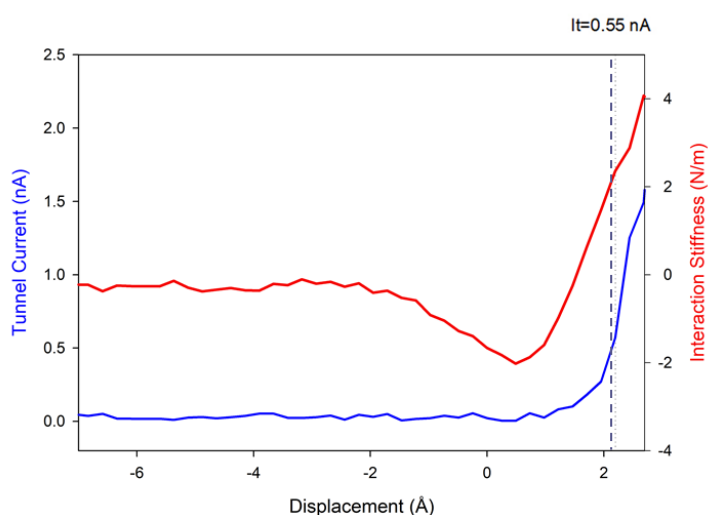
Later, the polycrystalline surface was sputtered with 1 keV beam energy and annealed at comparatively higher temperatures, 1100°C. This was conducted with the aim of obtaining a cleaner surface. However, the set parameters or the conditions of the tip and the sample surface were not sufficient to obtain atomic resolution images, specifically in force gradient channel.

4.1.3 Quantitative measurement of surface characteristics

In this section, force-distance spectroscopies obtained at different points on the polycrystalline diamond surface, using tungsten (W) and a highly boron doped diamond cantilevers are represented.

The particular force-distance spectroscopy on the polycrystalline diamond surface using tungsten (W) cantilever is shown in Figure 4.13. This measurement was acquired by using a sample bias voltage of -700 mV, which is in correlation with the set parameters of the atomic resolution images in Figure 4.12. The attractive and repulsive regimes are observed in the interaction stiffness. Furthermore, it is seen that the force interaction between the diamond surface and the tungsten tip comes earlier than the tunnel current. The dashed line indicates the set tunnel current used while scanning the surface. At this specific point on the surface, the interaction stiffness is positive at this tunnel current set point, which signifies that the force interaction is repulsive.

Figure 4.13 : Force-distance spectroscopy on polycrystalline diamond by using W cantilever, V_{bias}: -700 mV.

This force-distance spectroscopy in Figure 4.14 belongs to the polycrystalline sample, which was sputtered with 1 keV beam energy and annealed at 1100°C. This force-distance spectroscopy was acquired by using a sample bias voltage of -600 mV and tungsten (W) cantilever. As also seen in the graph, compared to the previous one in Figure 4.13, the force interaction and the tunnel current behaviors are synchronized in the manner of tip-sample distance. For example, around 0.55 nA tunnel current, the force interaction is no longer at repulsive regime, but in attractive regime. As stated before, this might be the probable reason of not being able to obtain atomic resolution imaging in force gradient channel, since the change of the interaction in repulsive regime is more intense compared to the attractive regime. In addition, it should be emphasized that there might be a tip change during this spectroscopy measurement, which only seems to affect the tunnel current.
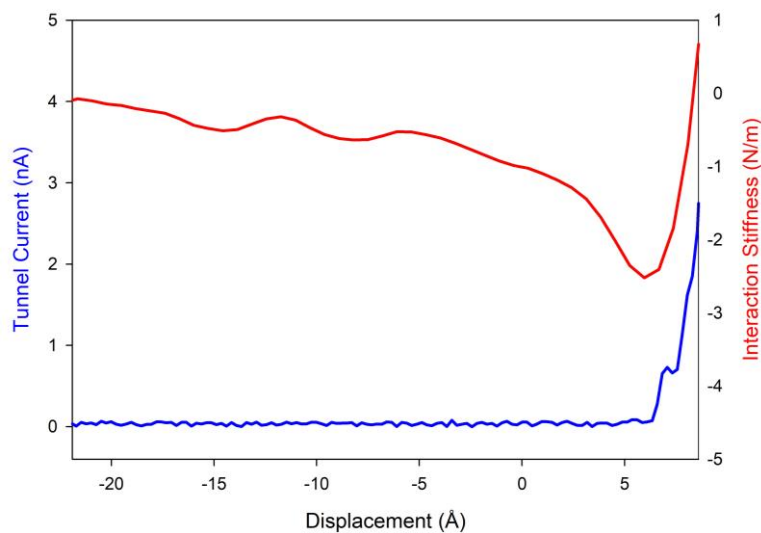
Figure 4.14 : Force-distance spectroscopy on polycrystalline diamond by using W cantilever, V_{bias}: -600 mV.

This specific force-distance spectroscopy in Figure 4.15, was accomplished using a highly boron doped diamond cantilever with stiffness of 70 N/m, by applying a sample bias voltage of 700 mV, on the same polycrystalline surface with the force-distance spectroscopy given in Figure 4.13. The main intention of this force-distance spectroscopy is measuring the force interaction and the tunnel current behavior between C-C atoms. At the first glance, the attractive region seems to have a longer range, compared to the tungsten cantilever. In spite of the tunnel current reaches to the values up to 12 nA, the force interaction does not proceed to repulsive regime. Similar to the previous measurement, this spectroscopy may demonstrate that

obtaining atomic resolution in force gradient channel could be challenging, since even at higher tunnel current values, the regime of interaction is attractive.
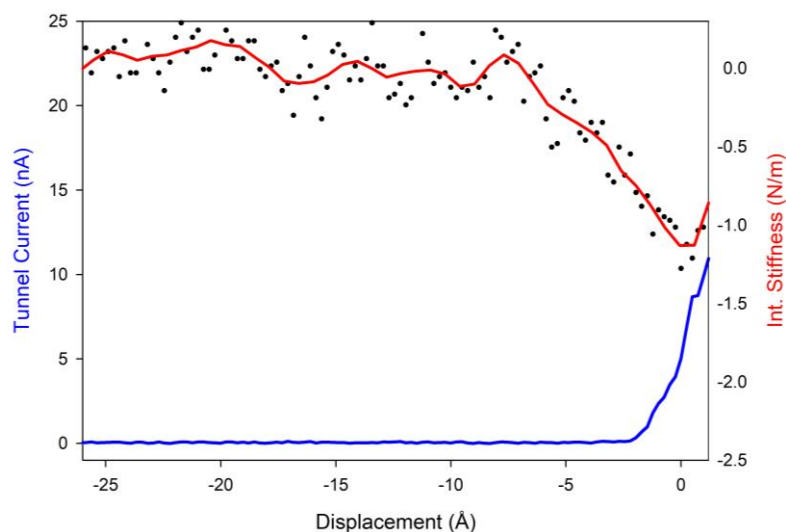
Figure 4.15 : Force-distance spectroscopy on polycrystalline diamond by using highly boron doped diamond cantilever, V_{bias}: 700 mV.

4.2 Single Crystalline Diamond Surface

The single crystalline diamond sample used in this work is a Ib <100> oriented sample, which has >200 ppm nitrogen concentration. The optical microscopy image of the single crystalline sample is shown in Figure 4.16. The extensively yellowish colour of the sample is a result of the high nitrogen doping.
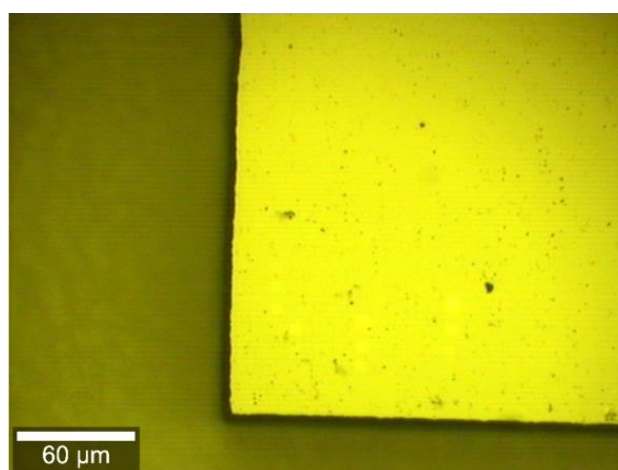
Figure 4.16 : Optical microscopy image of single crystalline diamond sample.

The sample was introduced to the UHV chamber after a wet cleaning process of acetone, isopropanol and distilled water. The large area scan of the surface shown in

Figure 4.17 demonstrate the initial surface, without any sputtering and annealing. High nitrogen doping might have led to obtaining tunnel current without any further cleaning procedure.
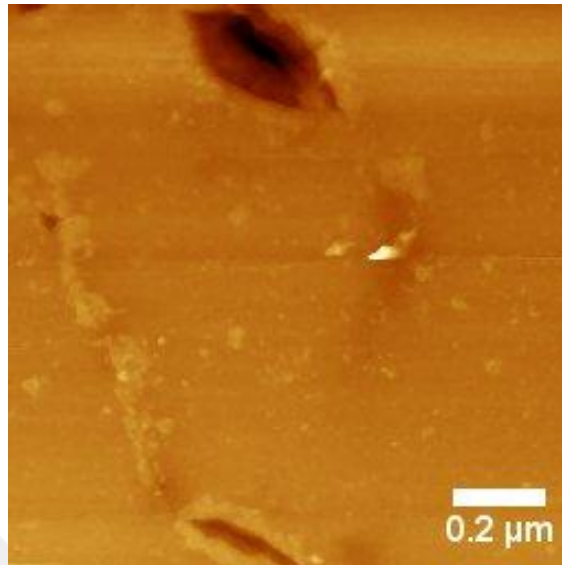
Figure 4.17 : UHV STM topography image of the single crystalline diamond surface with the set parameters V_{bias}: 7 V I_t: 0.25 nA.

However, the conditions were not sufficient for atomic resolution imaging on the single crystalline sample at this stage. This was supposed to be resulting from the contaminations on the surface. Thus, an acid etch procedure, which was mentioned in detail previously, was carried out. This was followed by the wet cleaning process including acetone, isopropanol and distilled water and the sample was introduced to the UHV chamber. Intriguingly, attaining tunnel current was harder, compared to the situation before the acid etch. It is thought that the main cause of this might be the excessive oxidation resulted by the acid etch.

In order to remove the oxidized layer from the surface, a gentle sputtering with sample plane oriented at 30° angle with respect to the sputter gun and subsequent annealing at 950°C was performed. In Figure 4.18, the large area scan of the surface after this process is seen. Comparatively, tunneling was obtained at lower bias voltages was achieved. Moreover, at the first sight, the surface topography has a flatter structure.
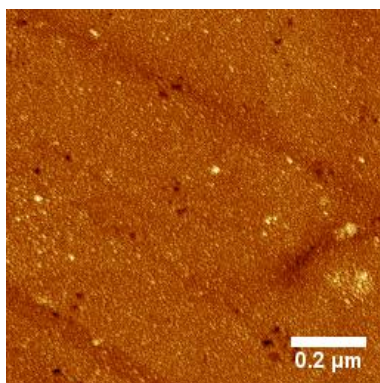
Figure 4.18 : UHV STM topography image of the single crystalline diamond surface with the set parameters V_{bias}: 700 mV I_t: 0.5 nA.

Simultaneously obtained STM/AFM results of a relatively large scan area are shown in Figure 4.19. In all channels, tunnel current modulation (measure of barrier height), oscillation amplitude (measure of force gradient), phase shift (measure of energy dissipation) and STM topography, a correlation can be observed.

In this scale of imaging, compared to the polycrystalline sample, there seems to be a much more ordered structure which is promising for atomic scale imaging.
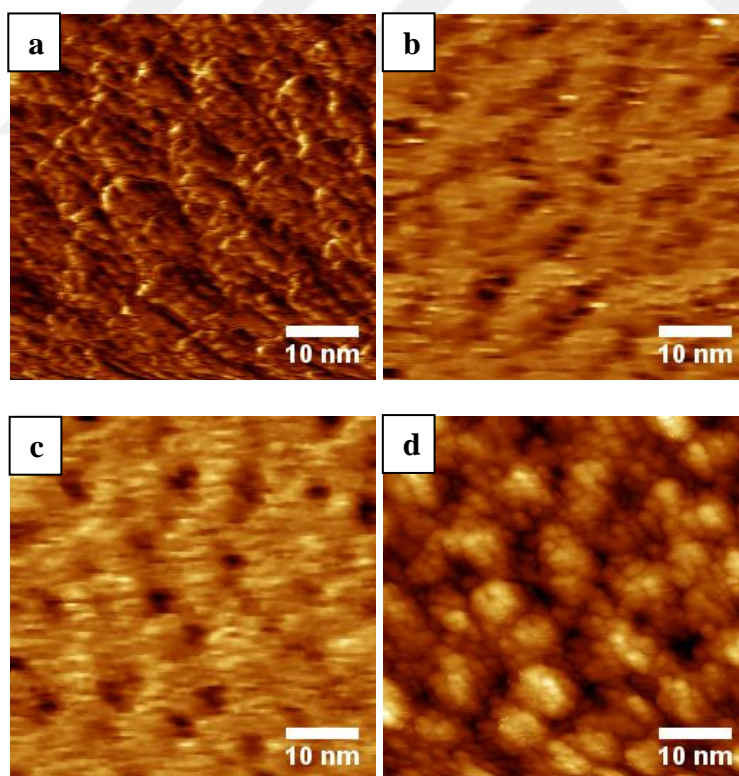
Figure 4.19 : UHV simultaneous STM/AFM images of the single crystalline diamond surface obtained by using W cantilever, with the set parameters V_{bias}: -500 mV. I_t: 1 nA $A_0 = 0.6$ Å$_{(p-p)}$ $f_0 =$ 31512 Hz $f =$ 19244 Hz (a) tunnel current modulation (b) interaction stiffness (c) phase shift (d) STM topography.

4.2.1 Atomic resolution imaging

In this section, the atomic resolution images of the single crystalline diamond surface are presented. The atomic resolution imaging was conducted by using a tungsten cantilever and a highly boron doped diamond cantilever.

The atomic resolution images shown in Figure 4.20 were achieved in tunnel current modulation (measure of barrier height), inverted oscillation amplitude (measure of force gradient), phase shift (measure of energy dissipation) and STM topography channels, using a tungsten cantilever. From the STM topography and comparing with results of other channels, it can be interpreted that the surface consists of regions with different heights, having similar crystallographic orientations.
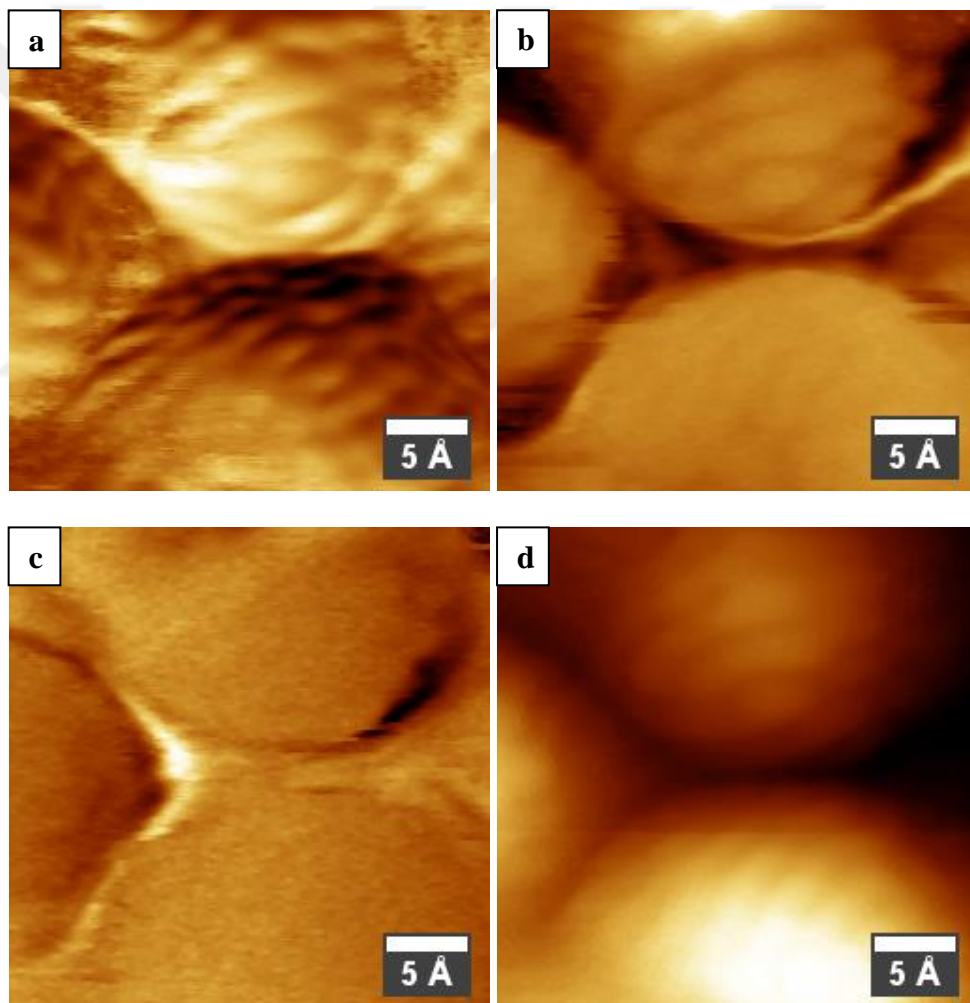

Figure 4.20 : UHV simultaneous STM/AFM images of the single crystalline diamond surface obtained by using W cantilever, with the set parameters V_{bias}: 500 mV. I_t: 2 nA $A_0 = 0.47$ Å$_{(p-p)}$ $f_0 = 31512$ Hz f $= 21940$ Hz (a) tunnel current modulation (b) interaction stiffness (c) phase shift (d) STM topography.

Another atomic resolution image of the same single crystalline surface is presented in Figure 4.21. A tungsten (W) lever with stiffness of 53 N/m was used to scan the surface. These results were obtained using comparatively higher values of set tunnel current and lower values of sample bias voltage, such as 2 nA and 500 mV respectively. As expected, a specific crystallographic structure is observed in this region. The scale bar indicates the periodicity of this structure to be approximately 2.5 Å (as indicated by the scale bar), which is in good agreement with the value given for (100) surface. For this region, the interaction stiffness and the barrier height were also studied in more detail. The calculated maximum barrier height value is 0.50 eV, as shown in Figure 4.21 (a). This range of barrier height is comparatively lower.

As shown in Figure 4.21 (b), the interaction stiffness for the same region was also calculated. The values for interaction stiffness are in the range of 1.04 N/m to 1.11 N/m. This demonstrates that during the whole period of scanning, the force interaction between the tip and the surface is repulsive.

In Figure 4.21 (c), the STM topography is shown. All three images of the same region are in a good agreement, when compared. The reason behind observing the periodic structures in small regions might be due to the partial cleaning of the surface, where amorphous phases could also exist in some regions.
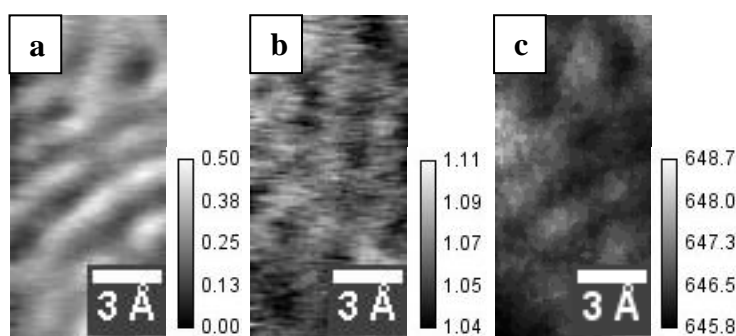

Figure 4.21 : UHV simultaneous STM/AFM images of the single crystalline diamond surface obtained by using W cantilever, with the set parameters V_{bias}: 500 mV. I_t: 2 nA $A_0 = 0.47$ Å $_{(p-p)}$ $f_0 = 31512$ Hz f $= 21940$ Hz (a) barrier height (b) interaction stiffness (c) STM topography.

In Figure 4.22, atomic resolution images obtained using highly boron doped diamond cantilever are shown. The tunnel current modulation (measure of barrier height), interaction stiffness and the STM topography are displayed. The periodic structure of (100) surface is barely seen in both tunnel current modulation and STM topography

images. A significant point to emphasize is that the sensitivity for the deflection detection of the cantilever oscillations was not sufficient to obtain atomic resolution in force gradient channel. This was mainly due to the fact that the reflectivity from the back of this particular cantilever was not efficient.
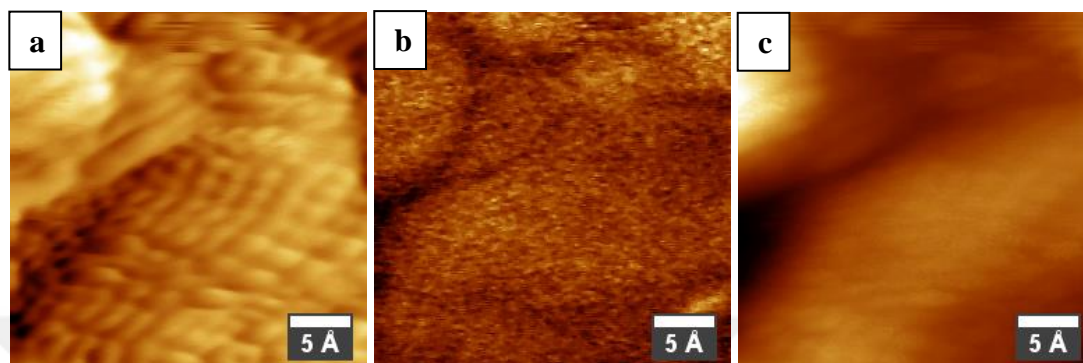
Figure 4.22 : UHV simultaneous STM/AFM images of the single crystalline diamond surface obtained by using highly boron doped diamond cantilever, with the set parameters V_{bias}: 500 mV. I_t: 0.35 nA $A_0 =$ 1.43 $\text{Å}_{(p-p)}$ $f_0 =$ 240430 Hz f = 27414 Hz (a) tunnel current modulation (b) interaction stiffness (c) STM topography.

Below, the results obtained using the highly boron doped diamond cantilever are displayed in Figure 4.23. For this region, the interaction stiffness and the barrier height were studied similar to the previous calculations. Figure 4.23 (a) shows the calculated barrier height, which has a range between 1.72 eV and 10.47 eV. As expected, compared to the calculations done on the same surface scans obtained with tungsten cantilever, the barrier height range is higher for the diamond cantilever.

The interaction stiffness for the same region was studied, as shown in Figure 4.23 (b). The values for interaction stiffness are in the range of 1.04 N/m to 1.12 N/m. This demonstrates that during the whole period of scanning, the force interaction between the tip and the surface is repulsive.

The STM topography is revealed in Figure 4.23 (c). In this region, the height corrugation indicated by the STM topography is 2.4 Å. All of the three channels show a consistent behavior when compared with each other.
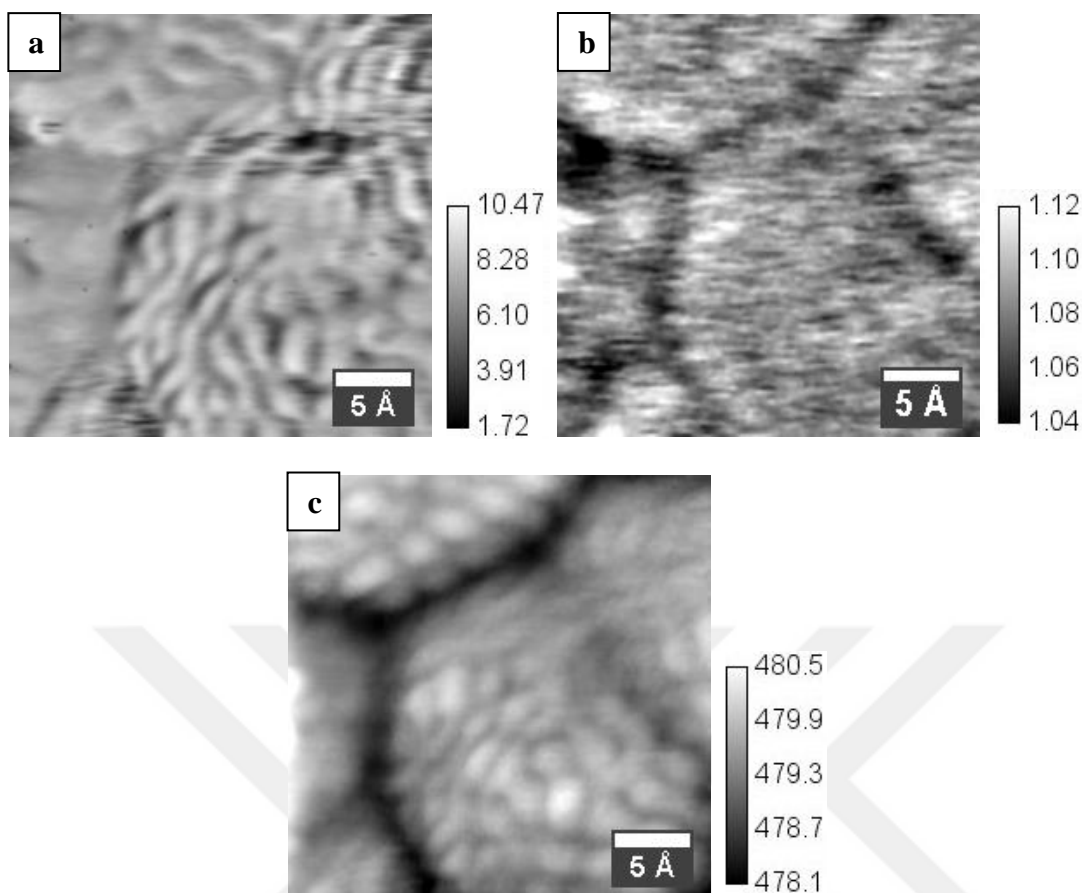
Figure 4.23 : UHV simultaneous STM/AFM images of the single crystalline diamond surface obtained using highly boron doped diamond cantilever, with the set parameters V_{bias}: -500 mV. I_t: 2.5 nA $A_0 = 2$ Å $_{(p-p)}$ $f_0 = 240430$ Hz $f = 27414$ Hz (a) barrier height (b) interaction stiffness (c) STM topography.

4.2.2 Quantitative measurement of surface characteristics

In this section, force-distance spectroscopies obtained at different points on the single crystalline diamond surface, using tungsten (W) and a highly boron doped diamond cantilevers are represented.

This following force-distance spectroscopy in Figure 4.24, was acquired using a highly boron doped diamond cantilever with stiffness of 70 N/m, by applying a sample bias voltage of 500 mV, on the single crystalline diamond surface. Identifying the force interaction and the tunnel current behavior between C-C atoms was aimed by this force-distance spectroscopy. This measurement is similar to the previous force-distance spectroscopy taken using the same diamond cantilever on polycrystalline diamond surface, which was given in Figure 4.15, in a manner of the tunnel current and force interaction behaviors related to the tip-surface distance.

Significantly, the force interaction does not reach the repulsive regime, even at the tunnel current values of 2.5 nA.
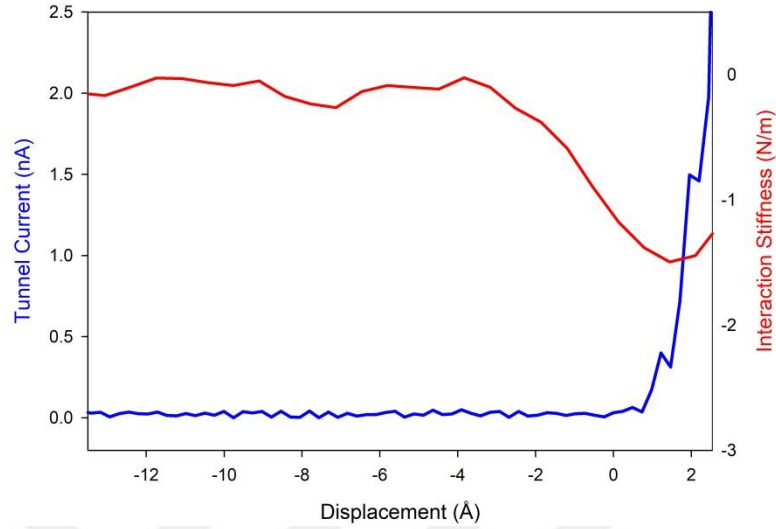
Figure 4.24 : Force-distance spectroscopy on single crystalline diamond by using highly boron doped diamond cantilever, V_{bias}: 500 mV.

In Figure 4.25, two separate force-distance spectroscopies conducted at the same point using two different bias voltages are presented. Using a tungsten tip on the single crystalline diamond surface, in order to investigate the effect of the applied sample bias voltage, two different bias voltage values, -1 V and 1 V were applied. First of all, it is observed that the attractive regime has a longer range for the case of V_{bias}:-1 V as seen in Figure 4.25 (a) compared to the V_{bias}:1 V, Figure 4.25 (b). The minimum value for the force interaction for V_{bias}:-1 V is two times of the minimum value for the force interaction measured for V_{bias}:1 V. Besides, it is known that the electrostatic force interaction, $k_{electrostatic}$, is related to the applied bias voltage and the contact potential as below:

$$k_{electrostatic} \propto (V_{bias} - V_{contact})^2 \qquad (4.1)$$

These results may imply that electrostatic force interaction is lower for the case that bias voltage is 1 V. Therefore, the contact potential could be suggested to have a value close to this bias voltage, 1 V.
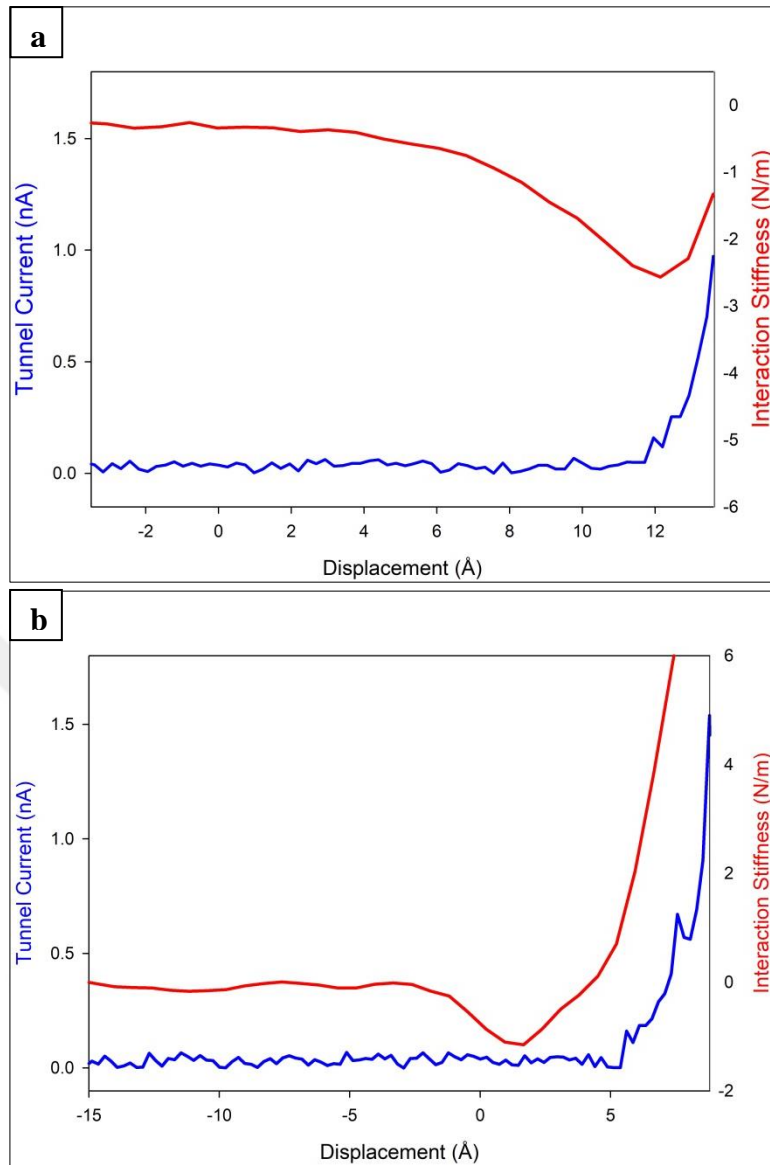
Figure 4.25 : Bias voltage dependent force-distance spectroscopies on single crystalline diamond by using tungsten cantilever, where applied sample bias voltage V_{bias} is (a) -1 V (b) 1 V.

5. CONCLUSION

In this study, the polycrystalline and single crystalline diamond surfaces have been investigated using simultaneous Scanning Tunneling/Atomic Force Microscopy in ultra-high vacuum (UHV). The surfaces were cleaned with the aim of obtaining atomically clean and flat surfaces, using various surface cleaning techniques including sputtering, annealing and acid etch. We used the tunnel current as the feedback parameter and oscillated the cantilever with sub-Ångström amplitudes at a specific frequency well below its resonance frequency. Using a fiber-optic interferometry setup, the changes in cantilever oscillation amplitudes were detected. This allowed the true simultaneous STM/AFM operation on the diamond surfaces, as being at certain operating regimes while scanning the surface.

The diamond surfaces were scanned using a Tungsten cantilever with a stiffness of 53 N/m and a highly boron doped diamond cantilever with a stiffness of 70 N/m, which were calibrated using thermal noise method. In this study, the surface topography of relatively smaller and larger areas on the polycrystalline and single crystal diamond surfaces were obtained. Moreover, the force, interaction stiffness, tunnel current modulation (measure of barrier height), phase shift (energy dissipation) and tunneling current information on the diamond surface were achieved. Atomic resolution imaging of diamond surface at different regions was accomplished. The surface structures of the different regions were discussed, since the atomic resolution images have shown areas with varying orientations. Furthermore, force-distance spectroscopy was conducted on different regions on the diamond surfaces, revealing the interaction stiffness between the diamond and the tip and the tunnel current behavior as well. This allowed maintaining quantitative measurement of the force interaction between two atoms of the diamond surface and the tip, as C-W and C-C. The maximum negative interaction stiffness between the polycrystalline diamond surface and the W tip is measured around -2-2.5 N/m, where the interaction stiffness between the polycrystalline diamond surface and the highly boron doped diamond tip is measured as -1.2 N/m. For the single crystalline diamond, the maximum negative interaction stiffness between the sample surface and the W tip is measured as -2.5 N/m and -1.2 N/m, with an applied bias voltage of -1 V and 1 V respectively. The maximum negative interaction stiffness between the single crystalline surface and the highly boron doped diamond tip is measured as -1.5 N/m.

REFERENCES

[1] **Neves, A. J. and Nazaré M. H.,** (2001) Properties, Growth and Applications of Diamond. 427

[2] **Everson, M. P. and Tamor, M. A.,** (1991) Studies of nucleation and growth morphology of boron-doped diamond microcrystals by STM, *J. Vac. Sci. Technol. B* **9** 1570–6

[3] **Zhang, L., Sakai, T., Yoshida, H., Yamanaka, S. and Okushi, H.,** (2002) Nanoscale characterization of hydrogenated and oxidized B-doped homoepitaxial diamond by conductive atomic force microscopy *J. Appl. Phys.* **91** 4585–9

[4] **Stallcup, R. E., Villarreal, L., Lim, S. C., Akwani, I., Aviles, A. F. and Perez, J. M.,** (1996(Atomic structure of the diamond (100) surface studied using scanning tunneling microscopy *J. Vac.* **14** 929–32

[5] **Stallcup, R. E. and Perez, J. M.,** (2002) Atomic structure of steps and defects on the clean diamond (100)-2×1 surface studied using ultrahigh vacuum scanning tunneling microscopy *Appl. Phys. Lett.* **81** 4538–40

[6] **Bobrov, K., Mayne, A., Comtet, G., Dujardin, G., Hellner, L. and Hoffman, A.,** (2003) Atomic-scale visualization and surface electronic structure of the hydrogenated diamond C(100)-(2×1):H surface *Phys. Rev. B - Condens. Matter Mater. Phys.* **68** 1–8

[7] **Tsuno, T., Tomikawa, T., Shikata, S. I. and Fujimori, N.,** (1994) Diamond homoepitaxial growth on (111) substrate investigated by scanning tunneling microscope *J. Appl. Phys.* **75** 1526–9

[8] **Baranauskas, V., Fukui, M., Rodrigues, C. R., Parizotto, N. and Trava-Airoldi, V. J.,** (1992) Direct observation of chemical vapor deposited diamond films by atomic force microscopy *Appl. Phys. Lett.* **60** 1567–9

[9] **Nimmrich, M., Kittelmann, M., Rahe, P., Mayne, A. J., Dujardin, G., Von Schmidsfeld, A., Reichling, M., Harneit, W. and Kühnle, A.,** (2010) Atomic-resolution imaging of clean and hydrogen-terminated C(100)- (2×1) diamond surfaces using noncontact AFM *Phys. Rev. B - Condens. Matter Mater. Phys.* **81** 1–4

[10] **Binnig, G. and Rohrer, H.,** (1982) Scanning tunneling microscopy *Nobel Lect.* **55** 726−735

[11] **Binnig, G. and Quate, C. F.,** (1986) Atomic Force Microscope *Phys. Rev. Lett.* **56** 930–3

[12] **Chen, C. J.,** (1993) *Introduction to scanning tunneling microscopy.* (Oxford Series in Optical & Imaging Sciences)

[13] **Voigtländer, B.,** (2015) *Scanning Probe Microscopy*

[14] **Garcia, R.,** (2010) *Amplitude Modulation Atomic Force Microscopy* (Wiley-VCH Verlag&Co. KGaA, Boschstr.)

[15] **Kittel, C. and Fan, H. Y.,** (1957) *Introduction to Solid State Physics* vol 25

[16] **Giessibl, F. J.,** (1998) High-speed force sensor for force microscopy and profilometry utilizing a quartz tuning fork *Appl. Phys. Lett.* **73** 3956–8

[17] **Oral, A., Grimble, R. A., Özer, H. Ö., and Pethica, J. B.,** (2003) High-sensitivity noncontact atomic force microscope/scanning tunneling microscope (nc AFM/STM) operating at subangstrom oscillation amplitudes for atomic resolution imaging and force spectroscopy *Rev. Sci. Instrum.* **74** 3656–63

[18] **Rugar, D., Mamin, H. J. and Guethner. P.,** (1989) Improved fiber-optic interferometer for atomic force microscopy *Appl. Phys. Lett.* **55** 2588–90

[19] **Fukuma, T.,** (2009) Wideband low-noise optical beam deflection sensor with photothermal excitation for liquid-environment atomic force microscopy *Rev. Sci. Instrum.* **80**

[20] **Anczykowski, B., Gotsmann, B., Fuchs, H., Cleveland, J. P. and Elings, V. B.,** (1999) How to measure energy dissipation in dynamic mode atomic force microscopy *Appl. Surf. Sci.* **140** 376–82

[21] **Lang, N.,** (1988) Apparent barrier height in scanning tunneling microscopy *Phys. Rev. B* **37** 10395–8

[22] **Fong, C. Y. and Klein, B. M.,** (1995) *Diamond: Electronic Properties and Applications* ed L S Pan and D R Kania (Boston, MA: Springer US)

[23] **Wort, C. J. H. and Balmer, R. S.,** (2008) Diamond as an *Rev. Lit. Arts Am.* **11** 22–8

[24] **Angus, J. C.,** (2014) Diamond synthesis by chemical vapor deposition: The early years *Diam. Relat. Mater.* **49** 77–86

[25] **Koizumi, S., Christoph, N. and Nesladek, M.,** (2008) *Physics and Applications of CVD Diamond*

[26] **Baumann, P. K. and Nemanich, R. J.,** (1998) Surface cleaning, electronic states and electron affinity of diamond (100), (111) and (110) surfaces *Surf. Sci.* **409** 320–35

[27] **Albarakaty, H. A.,** (2016) Fabrication of Graphene Electrodes on Diamond Substrate

[28] **Uzan-Saguy, C., Cytermann, C., Brener, R., Richter, V., Shaanan, M. and Kalish, R.,** (1995) Damage threshold for ion-beam induced graphitization of diamond *Appl. Phys. Lett.* **67** 1194

[29] **Baumann, P. K., Humphreys, T. and Nemanich, R.,** (1994) Comparison of surface cleaning processes for diamond C(001) *Materials Research Society Symposium - Proceedings* vol 339 pp 69–74

[30] **Hamza, A., Kubiak, G. and Stulen, R.,** (1990) Hydrogen chemisorption and the structure of the diamond C (100)-(2× 1) surface *Surf. Sci.* **237** 35–52

[31] **Holt, K. B., Bard, A. J., Show, Y. and Swain, G. M.,** (2004) Scanning electrochemical microscopy and conductive probe atomic force

microscopy studies of hydrogen-terminated boron-doped diamond electrodes with different doping levels *J. Phys. Chem. B* **108** 15117–27

[32] **Lettington, A. H., Tzeng, Y., Yoshikawa, M., Murakawa, M. and Feldman, A.,** (1991) *Applications of Diamond Films and Related Materials* vol 73

[33] **Xie, Z. Q., Bai, J., Zhou, Y., S., Gao, Y., Park, J., Guillemet, T., Jiang, L., Zeng, X. C. and Lu, Y. F.,** (2014) Control of crystallographic orientation in diamond synthesis through laser resonant vibrational excitation of precursor molecules *Sci. Rep.* **4** 1–7

CURRICULUM VITAE

Name Surname	**: İpen Demirel**
Place and Date of Birth	**: Konya / 27.09.1992**
E-Mail	**: demirelip@itu.edu.tr**

EDUCATION **:**

- **B.Sc.** **:** İstanbul Technical University, Physics Engineering

PROFESSIONAL EXPERIENCE AND REWARDS:

PUBLICATIONS, PRESENTATIONS AND PATENTS ON THE THESIS:

- **Demirel İ., Uluca A., Jadidi M.F., Özer H.Ö.** 2017: Construction of Ambient Simultaneous Scanning Tunneling/Atomic Force Microscope 81st Annual Meeting of the DPG and DPG Spring Meeting March 2017 Dresden, Germany

- **Demirel İ., Uluca A., Jadidi M.F., Özer H.Ö.** 2017: Construction of Ambient Simultaneous Scanning Tunneling/Atomic Force Microscope NanoTR13, 13rd Nanoscience and Nanotechnology Conference October 22-25, 2017 Antalya, Turkey

OTHER PUBLICATIONS, PRESENTATIONS AND PATENTS: